AGU ADVANCING EARTH AND SPACE SCIENCE

JGR Solid Earth

RESEARCH ARTICLE
10.1029/2019JB019005

The 1.24–1.21 Ga Licheng Large Igneous Province in the North China Craton: Implications for Paleogeographic Reconstruction

Chong Wang[1,2,3,4], Peng Peng[2,3], Zheng-Xiang Li[1], Sergei Pisarevsky[1,7], Steven Denyszyn[5], Yebo Liu[1], Hamed Gamal El Dien[1,6], and Xiangdong Su[2,3]

[1]Earth Dynamics Research Group, The Institute for Geoscience Research (TIGeR), School of Earth and Planetary Sciences, Curtin University, Western Australia, Australia, [2]State Key Laboratory of Lithospheric Evolution, Institute of Geology and Geophysics, Chinese Academy of Sciences, Beijing, China, [3]College of Earth and Planetary Sciences, University of Chinese Academy of Sciences, Beijing, China, [4]Department of Geosciences and Geography, University of Helsinki, Helsinki, Finland, [5]School of Earth Sciences, University of Western Australia, Western Australia, Australia, [6]Geology Department, Faculty of Science, Tanta University, Tanta, Egypt, [7]Institute of the Earth's Crust, Siberian Branch of the Russian Academy of Sciences, Irkutsk, Russia

Abstract Detailed geochronological, geochemical, and paleomagnetic studies of mafic dyke swarms, often associated with mantle plumes, can provide unique constraints on paleogeographic reconstructions. Mafic dykes with baddeleyite U–Pb ages of 1,233 ± 27 Ma (SIMS), 1,206.7 ± 1.7 Ma (TIMS), 1,214.0 ± 4.9 Ma (TIMS), and 1,236.3 ± 5.4 Ma (TIMS) have been identified in the eastern North China Craton. Geochemical data indicate subalkaline to alkaline basalt compositions with OIB-like trace element signatures and an intraplate tectonic setting. In addition to these geochemical signatures, the radiating geometry of these dykes also suggests a 1.24–1.21 Ga large igneous province caused by a mantle plume event. A new ~1.24 Ga paleomagnetic pole at 2.0°N, 165.1°E, A_{95} = 11.0°, N = 9 and an ~1.21 Ga VGP at −23.0°N, 92.5°E, dp/dm = 4.7°/7.8° have been obtained from these dykes, with the 1.24 Ga pole supported by positive baked contact test. Our paleomagnetic analyses suggest that the North China Craton and the proto-Australian continent could have been separated by 1.24–1.21 Ga from an established Nuna connection at ca. 1.32 Ga. By comparison with Laurentia paleopoles, we present the paleogeography of dispersing North China, proto-Australian, and Laurentia cratons in the late Mesoproterozoic during the breakup of the supercontinent Nuna.

Key Points:
- New 1.24–1.21 Ga Licheng large igneous province has been identified in the North China Craton
- A new key paleomagnetic pole of ~1.24 Ga has been obtained for the North China Craton
- Positions of North China, proto-Australian, and Laurentia cratons have been refined during Nuna breakup

Supporting Information:
- Supporting Information S1

Correspondence to:
C. Wang,
chong.wang1@postgrad.curtin.edu.au;
wangchong@mail.iggcas.ac.cn

Citation:
Wang, C., Peng, P., Li, Z.-X., Pisarevsky, S., Denyszyn, S., Liu, Y., et al. (2020). The 1.24–1.21 Ga Licheng large igneous province in the North China Craton: Implications for paleogeographic reconstruction. *Journal of Geophysical Research: Solid Earth*, *125*, e2019JB019005. https://doi.org/10.1029/2019JB019005

Received 7 NOV 2019
Accepted 29 MAR 2020
Accepted article online 6 APR 2020

1. Introduction

Three supercontinents have been hypothesized in Earth's history, that is, Pangea, Rodinia, and Nuna (also known as Columbia) (e.g., Li et al., 2008; Rogers & Santosh, 2002; Seton et al., 2012; Zhao et al., 2002). Among these, the configuration and evolution history of both Rodinia and Nuna are still controversial (Evans et al., 2016). Recent paleomagnetic and geological studies suggest that Nuna may have formed either at ~1.5–1.4 Ga (Meert & Santosh, 2017) or ~ 1.6 Ga (Furlanetto et al., 2013; Kirscher et al., 2019; Nordsvan et al., 2018; Pisarevsky, Elming, et al., 2014; Pourteau et al., 2018), much later than the previously proposed 2.0–1.8 Ga (Zhang, Li, et al., 2012; Zhao et al., 2002). However, its break-up process and timing are still poorly constrained, possibly starting by ~1.45–1.38 Ga (Pisarevsky, Elming, et al., 2014). Evans and Mitchell (2011) proposed that Nuna's core (Laurentia-Baltica-Siberia) broke up at some period between 1.50 and 1.25 Ga, marked by 1.38–1.35 Ga and 1.27 Ga magmatic events.

The North China Craton (NCC) was a part of Nuna, but paleogeographic reconstruction of the NCC in Nuna remains controversial (e.g., Hou et al., 2008; Peng, 2015; Wan et al., 2015; Zhang, Li, et al., 2012; Zhao et al., 2002). Zhang et al. (2017) have proposed a possible linkage between the northeast NCC and the northwest North Australian Craton (NAC) at ~1.32 Ga based on correlation of coeval radial mafic dyke swarms. It has also been recently proposed that the northeast NCC–northwest NAC connection can be dated back to ~1.78 Ga based on comparable apparent polar wander paths (APWPs) (Wang et al., 2019). This long-lived connection also finds support from multiple geological similarities, including comparable sedimentary basins and coeval ore deposits, microfossils, and magmatism (Wang et al., 2019). However, the dispersal of the northeast NCC from northwest NAC is less

constrained. Studies of late Mesoproterozoic mafic dyke swarms will provide critical information toward addressing this process.

Mafic dyke swarms refer to groups of linear mafic intrusions occurring either near parallel or radiating, representing a singular igneous episode (Ernst et al., 1995). They usually originate from mantle-derived magma and emplace over a short time interval (e.g., Ernst & Bleeker, 2010). They often act as magmatic channels for Large Igneous Provinces (LIPs), marking continental break-up events and providing a unique magmatic "barcode" for comparison among continental blocks in paleogeographic reconstructions (Bleeker & Ernst, 2006). Mafic dykes are also good targets for paleomagnetic studies, because they often hold stable and coherent magnetic remanence acquired during post-emplacement cooling and can be precisely dated (e.g., Halls et al., 2000). Here, we report new geochronological, geochemical, and paleomagnetic results of 1.24–1.21 Ga mafic dykes in the NCC. We also discuss the drift history of the NCC in the late Mesoproterozoic. Based on existing paleomagnetic data, we reconstruct the regional paleogeography in the context of break-up processes of the supercontinent Nuna.

2. Geological Background

The NCC is the oldest craton in China. It has been widely accepted that the NCC experienced orogeny at ~1.95–1.85 Ga according to high-pressure and ultrahigh-temperature granulite studies, although the precise ages of the orogenic events and extents of orogens remain debated (Kusky et al., 2007; Peng et al., 2014; Zhai & Santosh, 2011; Zhao et al., 2012). The final cratonization of the NCC occurred at ~1.8 Ga (Zhai, 2011). Four rift systems have developed following the cratonization, with ages ranging from the late Paleoproterozoic to the Neoproterozoic: the Yan–Liao, Zhaertai–Bayan Obo–Huade, Xiong'er, and Xu–Huai rift systems (Figure 1a).

The Yan–Liao rift is located in the northern part of the NCC (Figure 1a). It has two branches: one directed to the northeast and another to the interior of the NCC. This rift is mainly filled with ~1.7–1.6 Ga sandstones and shales (the Changcheng System); ~1.6–1.4 Ga carbonates (the Jixian System); ~1.4–>1.32 Ga clastic rocks (the Xiamaling Formation); and possibly Neoproterozoic clastic rocks (the Qingbaikou System) (Su et al., 2010). Additionally, several phases of magmatism have been reported in this area, including the ~1.75–1.68 Ga anorthosite–rapakivi granite suites intruding the Archean units (Yang et al., 2005; Zhang et al., 2007; Zhao, Chen, et al., 2004), 1.64–1.62 Ga volcanics accompanying the strata (Lu & Li, 1991; Zhang et al., 2013), ~1.32 Ga mafic sills intruding several formations (e.g., Zhang et al., 2017), and ~1.68 and ~1.23 Ga mafic dykes intruding the Archean basement (C. Wang et al., 2016; W. Wang et al., 2015). The E–W trending Zhaertai–Bayan Obo–Huade rift lies in the northern part of the NCC (Figure 1a). It contains four possibly synchronous groups outcropping in various places, that is, the Langshan, Zhaertai, Bayan Obo, and Huade groups from west to east. The sedimentary sequences are metamorphosed to low grades. Some of the strata have recently been dated, with ages ranging from late Paleoproterozoic to the Neoproterozoic (e.g., Liu et al., 2017). The Xiong'er rift lies in the southern part of the NCC (Figure 1a). It has three branches: two along the southern margins and one toward the interior of the NCC. This rift contains mainly clastic deposits (the ~1.8–1.6 Ga Xiong'er, Ruyang, and Luoyu groups) and carbonates (the <1.6 Ga Guandaokou Group). The 1.78 Ga volcanics are developed within the Xiong'er rift (Zhao, Zhai, et al., 2004). These volcanics may be part of a LIP including a coeval giant mafic dyke swarm (Peng et al., 2008). The Xu–Huai rift lies in the southeastern part of the NCC (Figure 1a). This rift mainly developed in the early Neoproterozoic (He et al., 2017). Notably, 0.92–0.89 Ga mafic sills are emplaced into several sedimentary formations associated with this rift (e.g., Peng, Bleeker, et al., 2011; Zhang et al., 2016).

Several episodes of Precambrian mafic magmatism have been reported from the NCC, including events at 1.78, 1.73, 1.68, 1.62, 1.32, 1.23, 0.92–0.89, and 0.81 Ga (Peng, 2015). Among these, the 1.78, 1.32, and 0.92–0.89 Ga events have been most extensively studied (e.g., Peng et al., 2008, Peng, Bleeker, et al., 2011, Peng, Zhai, et al., 2011; Zhang et al., 2016, 2017).

Wang et al. (2015) reported several NE-trending aprroximately 1.23 Ga mafic dykes in the northern Jidong and Jianping areas (Figure 1d) and suggested that the widespread 1.27–1.21 Ga magmatism represents a mantle plume event correlated with similar-aged events in several continents. The U–Pb SIMS baddeleyite age of the Licheng dyke swarm in central NCC is 1,229 ± 4 Ma (Peng, 2015), and ages of two dykes in the Jidong area are 1,228 ± 4 and 1,236 ± 7 Ma (weighted-mean $^{207}Pb/^{206}Pb$ ages) (Wang et al., 2016;

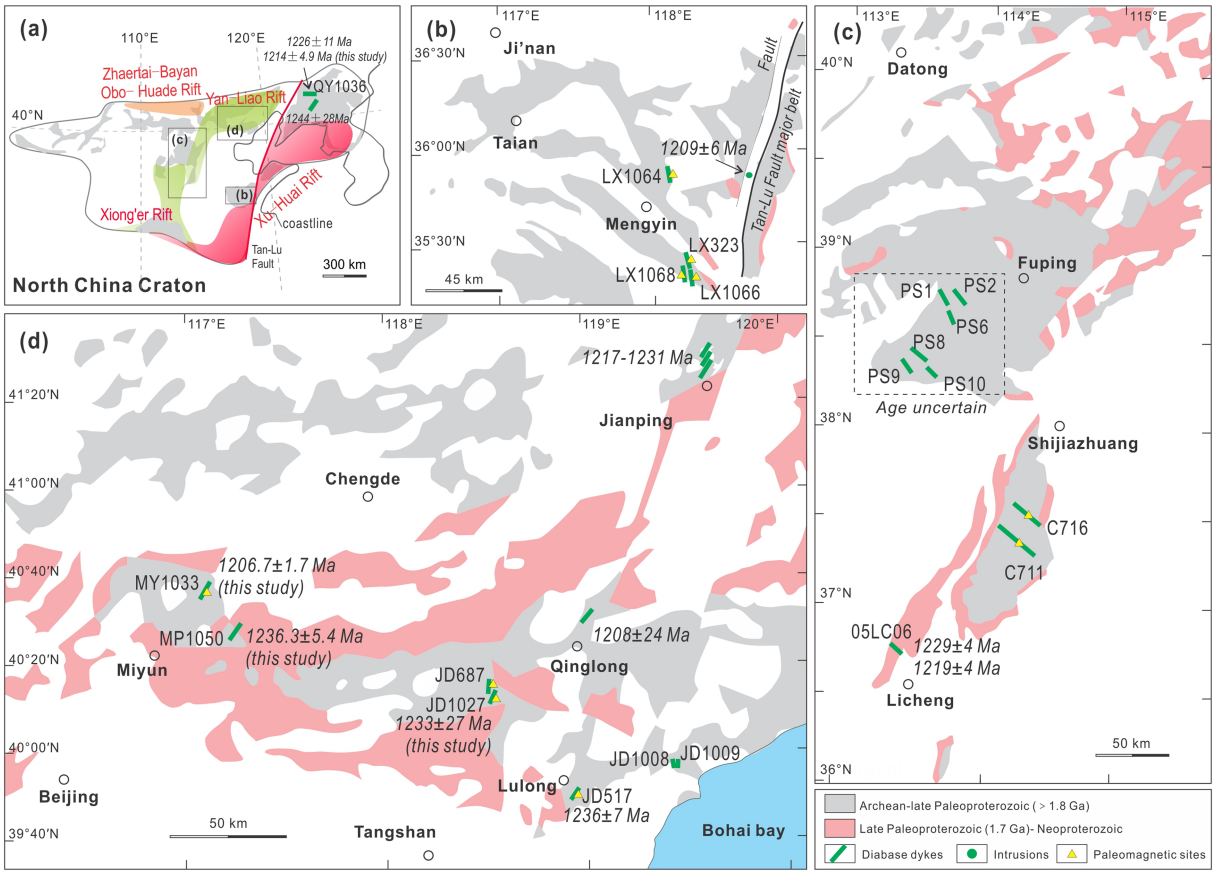

Figure 1. Schematic geological maps: (a) Proterozoic rifts of the NCC and locations of study regions; distribution of the 1.24–1.21 Ga mafic dykes/intrusions in (b) Luxi, (c) central NCC, and (d) Jidong. Position of the Qingyuan dyke (QY1036) near the eastern Tan-Lu fault is shown in (a). The PS dykes in (c) are from Ding (2017). Age references are in Table 1.

Xiang, 2014) (Figures 1c and 1d). In addition, one gabbro intrusion with a U–Pb SHRIMP zircon age of 1,209 ± 6 Ma ($^{207}Pb/^{206}Pb$ age) has been reported from Yishui, Luxi region (Figure 1b; Peng et al., 2013), and two dykes with U–Pb LA-ICPMS zircon ages of 1,244 ± 28 Ma (upper intercept age) and 1,226 ± 11 Ma ($^{207}Pb/^{206}Pb$ age) were from the east Tan-Lu fault (northeast NCC) (Figure 1a; Pei et al., 2013; Wang et al., 2015). In this study, we regard all these intrusions as belonging to the same magmatic event because of their near coeval ages (Table 1), as well as geochemical and paleomagnetic characteristics (see below).

3. Field Observations, Petrography and Sampling

Most studied dykes intrude Archean basement (Figure 1b–1d). The geological map shows that the Mipu dyke (MP1050) intrudes the ~1.56 Ga Gaoyuzhuang Formation and the older Changcheng Group in the Yan–Liao rift. However, their relationship is hard to identify in the field because of heavy vegetation cover and weathering (Figure 1d). These dykes show varying trends (Figures 1b–1d).

In the Jidong area, the Laowangjia dyke at Taipingzhai Town, Qianxi County (JD1027; Figure 1d) is located adjacent to the previously studied Laolijia dyke (JD687; Wang et al., 2016). The Laowangjia dyke (about 24° strike and ~30 m wide) intrudes Archean gneisses, exhibiting clear but weathered and fragmented chilled margins. The interior part of this dyke has a coarse granular texture (Figure 2a. The Xitongye (JD1008) and Dongtongye (JD1009) dykes show ~N-S trends (striking ~350–002°, azimuth directions). The exposed part of the JD1009 dyke is ~10 m wide, but its margin is not exposed. The studied rocks in the Jidong area mainly consist of plagioclase (50–55%) and pyroxene (35–40%) with minor amount of biotite, Fe-Ti oxides, and zircon (Figures 2g and 2h). The Baihejian dyke (MY1033) is located northeast of the Miyun town

Table 1
Summary Information of 1.24–1.21 Ga Magmatism in the NCC

Location	Occurrence	Trend	Ages/Ma	Method	Reference
Yishui, Luxi	Intrusion	----	1,209 ± 6	Zr-S	Peng et al., 2013
Tonghua, Jilin*	Dyke	NE	1,244 ± 28	Zr-L	Pei et al., 2013
Jianping, Liaoxi	Dyke-S	38°	1,229 ± 10	Zr-L	Wang et al., 2015
			1,217 ± 13	Zr-S	Ding, 2017
	Dyke-M	38°	1,229 ± 4	Zr-L	Wang et al., 2015
			1,231 ± 16		
			1,226.9 ± 3.4	Zr-S	Ding, 2017
	Dyke-N	38°	1,222.9 ± 6.1	Zr-S	Ding, 2017
Qingyuan, Liaobei*	Dyke	EW	1,226 ± 11	Zr-L	Wang et al., 2015
			1,214.0 ± 4.9	Bd-T	This study
Qinglong, Jidong	Dyke	40°	1,208 ± 24	Zr-L	Wang et al., 2015
Luannan, Jidong	stock, dyke?	----	1,228 ± 4	Bd-S	Xiang, 2014
Licheng	Dyke	NW	1,229 ± 4	Bd-S	Peng, 2015
			1,219.1 ± 4.3	Bd-S	Ding, 2017
Lulong, Qinhuangdao	Dyke	32°	1,236 ± 7	Bd-S	Wang et al., 2016
Qianxi, Tangshan	Dyke	32°	1,233 ± 27	Bd-S	This study
Baihejian, Miyun, Beijing	Dyke	30°	1,206.7 ± 1.7	Bd-T	This study
Mipu, Xinglong, Chengde	Dyke	NE	1,236.3 ± 5.4	Bd-T	This study

Note. Locations marked "*" represent to the eastern Tan-Lu fault belt. Zr-zircon, Bd-baddeleyite; S, L, and T represent SIMS, LA-ICPMS, and TIMS methods.

(Figure 1d). This dyke has a 35° strike and is approximately 80 m wide with clear chilled margins (Figure 2b). The rocks are diabase with ophitic texture (Figure 2i). The Mipu dyke (MP1050) is located at southeast of dyke MY1033, in Xinglong Town, Chengde City. This dyke trends NE. The rocks are coarse grained and weathered.

In the central NCC, two dykes (C711 and C716; Figure 1c) intruded the Archean units. These dykes are over 15 m wide and are NW trending (~310°). Spheroidal weathering is ubiquitous (Figure 2d). These rocks are composed of plagioclase (~50%) and pyroxene (~40%), with hornblende (2–5%), biotite (2–5%), and Fe-Ti oxides (~5%) (Figure 2j, k).

In the Luxi area (Figure 1b), four studied dykes (LX323, LX1064, LX1066, and LX1068) show NNW trends (~352°) and are between 10 and 20 m wide. Chilled margins are easily identifiable along contacts with the host granites (Figure 2f). The Jiaopo dyke (LX1064) has been petrographically described by Wang et al. (2007). It consists of ~40% clinopyroxene and ~50% plagioclase with minor hornblende, biotite, quartz, and chlorite (sample 05SD-21). In general, the plagioclase grains in these dykes are over 1 mm in length, with various degrees of saussuritization (Figures 2g–2l). Clinopyroxene is fresh and small compared to plagioclase (Figures 2g–2l). Fe-Ti oxides are usually 0.1–0.5 mm in size and exist as euhedral crystals within plagioclase and clinopyroxene groundmass (Figures 2g–2l).

For geochronological analyses, baddeleyites were extracted from the Baihejian (MY1033), Mipu (MP1050), and Laowangjia (JD1027) dykes of the Jidong region (Figure 1d). Additionally, one dyke in Qingyuan, northern Liaoning province (sample 12LN54-1; Wang et al., 2015) is redated by using the baddeleyite U–Pb ID-TIMS method (dyke QY1036; Figure 1a). Samples for geochemical analyses were collected from the Laowangjia (JD1027), Xitongye (JD1008), and Dongtongye (JD1009) dykes of the Jidong area (Figure 1d), from the Wucaizhuang (LX323), Jiaopo (LX1064), Xiayandian (LX1066), and Gaojiaweizi (LX1068) dykes of the Luxi area (Figure 1b) and from the Renjiadong (C716) and Nangou (C711) dykes of the central NCC (Figure 1c).

For the paleomagnetic study, 10 dykes have been drilled (Figure 1), excluding the Xitongye, Mipu, and Qingyuan dykes (JD1008, MP1050, and QY1036) mostly due to poor outcropping but including the Laolijia dyke (JD687) and 1,236 ± 7 Ma Maojiagou dyke (JD517) in Jidong (Figure 1d) (Wang et al., 2016). For each dyke (treated as one site), 7–15 oriented samples were collected from scattered outcrops. Samples were oriented using sun compass for sites MY1033, JD1027, JD687, JD517, LX323, LX1064, C711, and C716 (except sites LX1066 and LX1068). All samples were oriented using a magnetic compass. In the

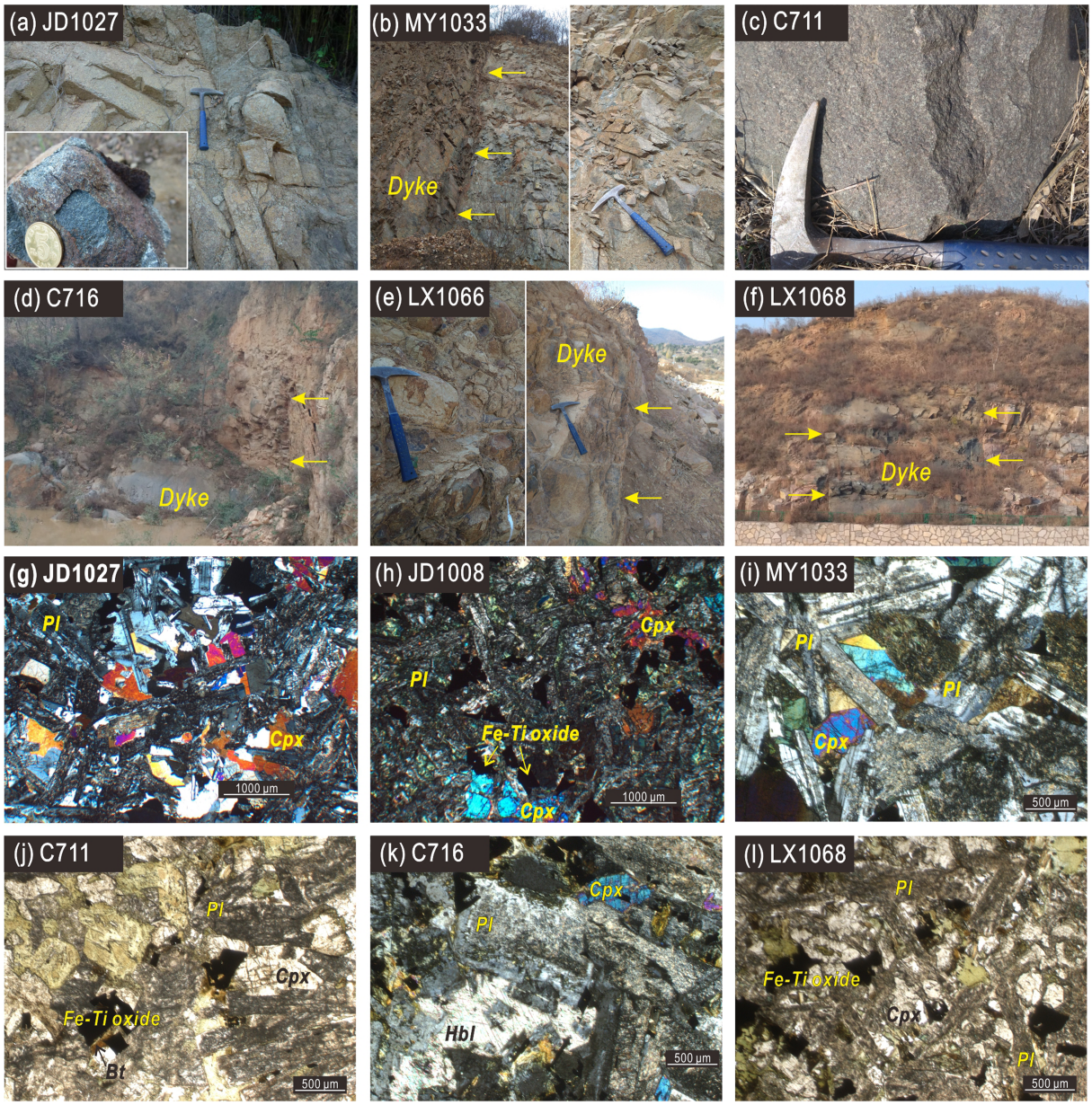

Figure 2. Representative photos of outcrops and block samples (a–f) and thin sections microphotographs (g–l). Arrows in (b, d–f) indicate (near) vertical and regular boundaries between mafic dykes and country rocks. Pl-plagioclase, Cpx-clinopyroxene, Hbl-hornblende, Bt-biotite. Microphotographs (j) and (l) are under single polarized, and (g–i) and (k) are under cross polarized lights.

field, the needle of magnetic compass shows insignificant changes when approaching the surface of dyke bodies, indicating the reliability of magnetic compass readings. The azimuths determined between magnetic and sun compasses show few differences (<5°).

4. Analytical Methods

4.1. Geochronology

Standard density and magnetic techniques were used for baddeleyite separation from rock powders at the Yu'neng Geological and Mineral Separation Survey Centre, Langfang City, and the Institute of Geology and Geophysics, Chinese Academy of Sciences (IGGCAS). The U–Pb dating of sample 1027LWJ1 was carried out on a CAMECA SIMS 1280HR facility at the IGGCAS, following procedures described by Li

et al. (2009). Before measurement baddeleyite grains, together with Phalaborwa baddeleyite standards, were fixed and polished on a 2.5 cm diameter resin disk, then observed by transmitted and reflected photomicrographs, followed by backscattered electron (BSE) images that were obtained by a field emission scanning electron microscopy (Nova NanoSEM 450) at IGGCAS. After imaging, the disk was coated with high purity gold. Analyses were carried out using an O_2^- primary beam accelerated at −13 kV with spot size of approximately 30 × 20 μm or smaller. To reduce the baddeleyite U/Pb orientation effect (Wingate & Compston, 2000), we adopt the oxygen flooding technique for measurement of the Pb isotopes (Li et al., 2010). Crystals of Phalaborwa baddeleyite were measured to check Pb isotope fractionation (Heaman, 2009; Li et al., 2010). Oxygen flooding can also enhance the yield of secondary Pb^+ ions (Li et al., 2010). Non-radiogenic ^{204}Pb from contemporary crust is used for correcting the raw data (Stacey & Kramers, 1975).

U–Pb dating of samples 1033BHJ1, 1036QY1, and 1050MP1 was carried out on a Thermo Triton Plus mass spectrometer at the TIMS facility of the Curtin University, Australia. No pretreatment methods were used beyond cleaning the grains with concentrated distilled HNO_3 and HCl, and due to their small size, no chemical separation methods were required. Before measurement, the samples were spiked with an in-house ^{205}Pb-^{235}U tracer solution and dissolved in the clean-lab facilities of the University of Western Australia. Dissolution and equilibration of spiked single crystals were by vapor transfer of HF, using Teflon microcapsules in a Parr pressure vessel placed in a 230 °C oven for 6 days. The resulting residue was redissolved in HCl and H_3PO_4 and placed on an outgassed, zone-refined rhenium single filament with 5 μL of silicic acid gel. Uranium was measured as an oxide (UO_2). Fractionation was monitored using SRM981 and SRM982. Mass fractionation was 0.04 ± 0.09%/amu, and U decay constants used were from Jaffey et al. (1971). The weights of the baddeleyite crystals were calculated from measurements of photomicrographs and estimates of the third dimension. Data were reduced and plotted using the software packages Tripoli (from CIRDLES.org) and Isoplot 4.15 (Ludwig, 2012).

4.2. Geochemistry

Representative samples were ground into powder using a disc mill at the IGGCAS. The whole-rock major and trace elements measurements were carried out at the IGGCAS (including dykes of JD1008, JD1009, JD1027, and C716) and the ALS Minerals–ALS Chemex (Guangzhou) Co Ltd (including dykes of C711, LX323, LX1064, LX1066, and LX1068). The loss on ignition (LOI) was determined as the weight loss after 1 hour's baking at constant 1,000 °C. Powdered samples were mixed with lithium tetraborate and cosolvent into fused disks and then analyzed by X-ray fluorescence AXIOS Minerals (IGG) and PANalytical PW2424 (ALS). Precision was better than 5%.

At the IGG, samples for trace-element analyses were digested in acid (HNO_3 + HF) for 7 days at 200 °C, then measured by Inductively Coupled Plasma Mass Spectrometry (ICP-MS) Element. At the ALS, samples for trace-element analyses were dissolved at high temperature (>1,025 °C) with lithium metaborate/lithium tetraborate, then fixed volume by HNO_3 + HCl + HF and measured by an ICPMS Agilent 7700x. While, for Cr and Ni analyses at the ALS, the samples were dissolved by $HClO_4$ + HNO_3 + HF, then fixed volume by HCl, and measured by an ICPMS Agilent 7900. The relative standard deviation was better than 10%.

4.3. Rock Magnetism, Magnetic Fabric, and Paleomagnetism

Rock magnetic analyses include thermal-magnetic experiments (κ-T curves) and progressive thermal demagnetization of triaxially orthogonal isothermal remanent magnetization (IRM) (Lowrie, 1990). κ-T curves were obtained from uniform powders on a kappabridge susceptibility meter (MFK1-FA) linked with a CS4 furnace. Besides, representative samples have been magnetically saturated along three mutually orthogonal axes by 0.12, 0.4, and 3.0 T, then thermally demagnetized in the Magnetic Measurements Thermal Demagnetizer (MMTD) and measured in a JR-6A spinner magnetometer. Anisotropy of magnetic susceptibility (AMS) was measured with the MFK1-FA before demagnetization. Magnetic-fabric data were plotted using the Anisoft5 software.

Most specimens were put through progressive thermal demagnetization, and some were applied to the alternating field (AF) demagnetization. Thermal demagnetization was conducted in about 17 steps from 100 °C to 580 °C using an ASC TD-48SC and a MMTD. The remanent magnetization has been measured in a magnetically shielded room with a 2G 755 superconducting rock magnetometer with a vertical Model 855 automated sample handler (magnetic moment of (2.09 ± 0.72) × 10^{-10} Am^2), though sometimes a spinner

magnetometer JR-6A was used. Remanence vectors were computed by principal component analysis (Kirschvink, 1980) with a maximum angle of deviation (MAD) less than 10° for all the samples, and site-mean directions were calculated directly by stable endpoints with the PuffinPlot software (Lurcock & Wilson, 2012). Paleogeographic reconstructions were built with the GPlates free software (http://www.gplates.org/). All analyses have been carried out at Curtin University, Australia.

5. Results

5.1. Geochronological Results

About 40 baddeleyite crystals were isolated from 20 kg of sample 1027LWJ1 (40.245°N, 118.486°E; Laowangjia dyke-JD1027; Figure 1d). These crystals have a tabular shape (50–80 μm × 10–20 μm) and are brownish in color (Figure 3a). Only six spots (from six grains) were analyzed by SIMS due to the small size of the crystals. $^{206}Pb/^{204}Pb$ ratios range from 1,069 to 47,966. Four have $^{207}Pb/^{206}Pb$ apparent ages of 1,202–1,246 Ma (Figure 3a; Table S1). Six analyses yield a weighted-mean $^{207}Pb/^{206}Pb$ age of 1,233 ± 27 Ma (MSWD = 0.55) (Figure 3a). No microcrystalline zircon coatings were observed around these baddeleyites, so the high uncertainties for the two spots could arise from common ^{204}Pb contamination during analyses, possibly resulting from beam diameters (30 × 20 μm) significantly overlapping the crystal's edge (spot 3) or internal fissures (spot 6) (Figure 3a). Nevertheless, given the overall coherence of the $^{207}Pb/^{206}Pb$ age, we argue that the ~1,233 Ma age represents the crystallization age of this dyke.

For U–Pb ID-TIMS analysis, five small baddeleyite crystals were analyzed from sample 1033BHJ1, Miyun town (40.617°N, 117.083°E; dyke MY1033; Figure 1d and Table S2). Calculated U concentrations were between 85 and 218 ppm. The data are variably discordant (Figure 3b), indicating some degree of Pb loss, probably largely from the microcrystalline zircon overgrowths. The coherence of the $^{207}Pb/^{206}Pb$ dates indicates that Pb loss was recent, further supported by a free regression of all data yielding upper and lower intercepts at 1,204.3 ± 4.0 and −60 ± 98 Ma, respectively. Recent Pb loss permits use of the weighted-mean $^{207}Pb/^{206}Pb$ age to represent the magmatic emplacement age of the dyke. The weighted-mean $^{207}Pb/^{206}Pb$ age of all five analyses is 1,206.7 ± 1.7 Ma (MSWD = 1.09).

Six single baddeleyite grains were analyzed from sample 1036QY1, Qingyuan (42.139°N, 124.951°E; dyke QY1036; Figure 1a and Table S2). The grains are rather small, with calculated weights of about 0.2 μg and calculated U concentrations between 178 and 276 ppm. As with the sample 1033BHJ1, frostings of microcrystalline zircon are considered the source of analyzed material that has lost Pb, resulting in four of six fractions being variably discordant, though two fractions yielded concordant data (Figure 3c). Upper and lower intercept ages from a free regression are 1,215.5 ± 7.2 and 79 ± 250 Ma, respectively; the zero-age lower intercept and a coherent set of $^{207}Pb/^{206}Pb$ dates again indicate that Pb loss was recent, and the weighted-mean $^{207}Pb/^{206}Pb$ age of all six analyses is 1,214.0 ± 4.9 Ma (MSWD = 0.49). We consider this to represent the magmatic emplacement age for this dyke.

Four baddeleyite grains were analyzed from sample 1050MP1, Mipu dyke (40.443°N, 117.254°E; MP1050; Figure 1d and Table S2). U concentrations range from 139 to 198 ppm. Three sets of data are near concordant (Figure 3d), with a free regression yielding upper and lower intercept ages of 1,235.6 ± 5.0 Ma and −506 ± 2,500 Ma, respectively, the latter indicating any Pb loss to be recent. The weighted-mean $^{207}Pb/^{206}Pb$ age of all analyses is 1,236.3 ± 5.4 Ma (MSWD = 0.2), which we consider to be the magmatic emplacement age.

5.2. Geochemical Results

Whole rock major and trace elements from nine dykes are reported (Table S3). Most samples plot in subalkaline to alkaline basaltic fields in element classification diagrams (Figure 4). These dykes show a narrow range of SiO_2 contents (48.4–53.2 wt.%) and MgO contents (4.38–6.22 wt.%). The rocks are characterized by high TiO_2 content (>1.61 wt.%), moderate total iron (tFe_2O_3 content of 11.0–14.7 wt.%), with $Na_2O + K_2O$ content of 3.34–6.22 wt.% (Table S3). The Mg# values are 42.0–52.7 ($Mg\# = 100 \times Mg/(Fe^{2+}_{total} + Mg)$, in molecular; Table S3). Compatible elements such as Cr and Ni are 28–336 ppm and 48–93 ppm, respectively (Figures 5f and 5g). In summary, the MgO show linear trends with SiO_2, CaO, La, Th, and Nb (Figure 5).

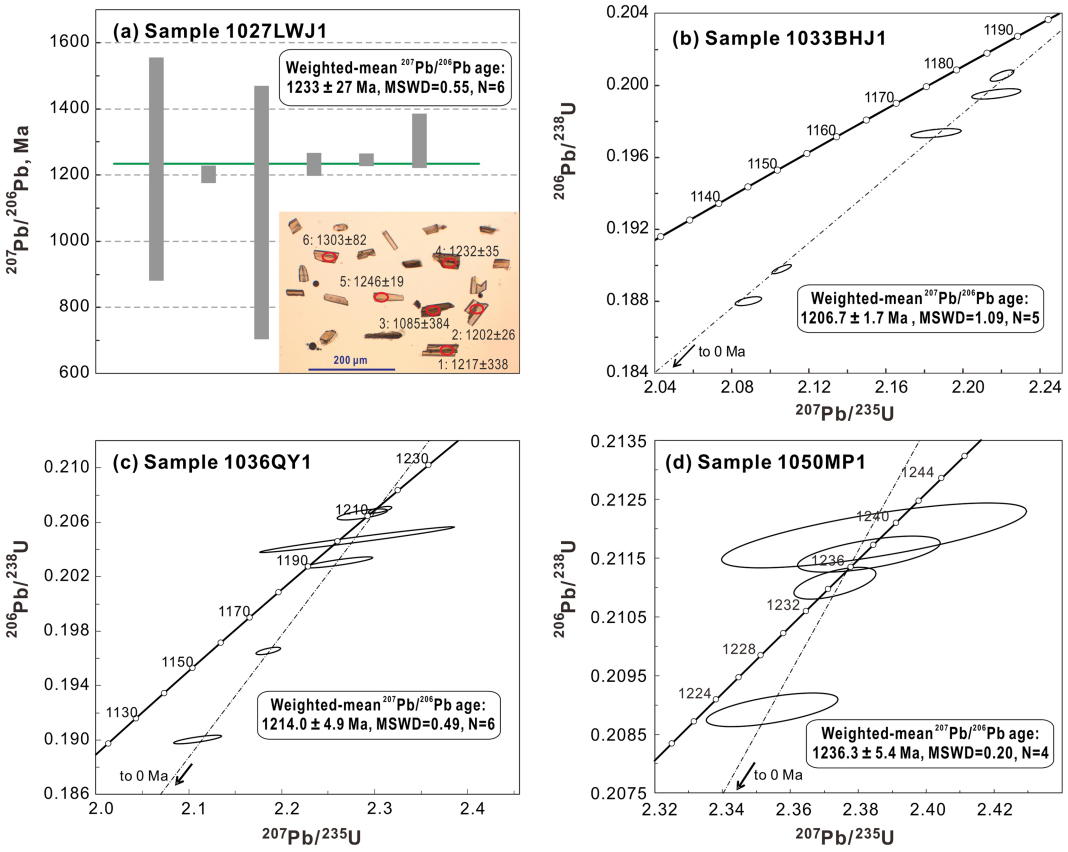

Figure 3. Baddeleyite dating results of mafic dykes. (a) Sample 1027LWJ1 from Laowangjia dyke (JD1027) with mineral picture under transmitted light; (b) sample 1033BHJ1 from Baihejian dyke (MY1033); (c) sample 1036QY1 from Qingyuan dyke (QY1036); and (d) sample 1050MP1 from Mipu dyke (MP1050).

The studied rocks show moderate to high total rare earth element compositions (ΣREE = 107–235 ppm) with enriched light REEs (La/Yb_N = 6.15–18.6, Chondrite-normalized value), and minor to strikingly positive Eu anomalies ($Eu/Eu^* = Eu_N/[(Sm_N) \times (Gd_N)]^{1/2}$, values of 0.97–1.73) (Figure 6a). On the primitive mantle normalized trace element spider diagrams, Nb presents negative anomaly relative to Th and La, while Ti in most samples exhibits as negative anomalies relative to Zr and Gd (Figure 6b).

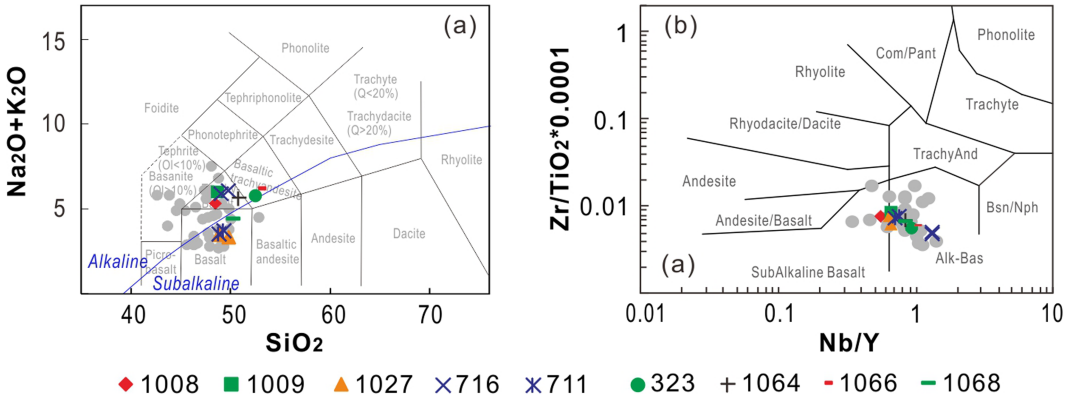

Figure 4. Element geochemical classification of the dykes. (a) TAS diagram; (b) Zr/TiO_2 * 0.0001 vs. Nb/Y diagram (after Winchester & Floyd, 1977). Gray dots represent compiled data for the dated 1.24–1.21 Ga mafic intrusions (N = 37) (Table S5).

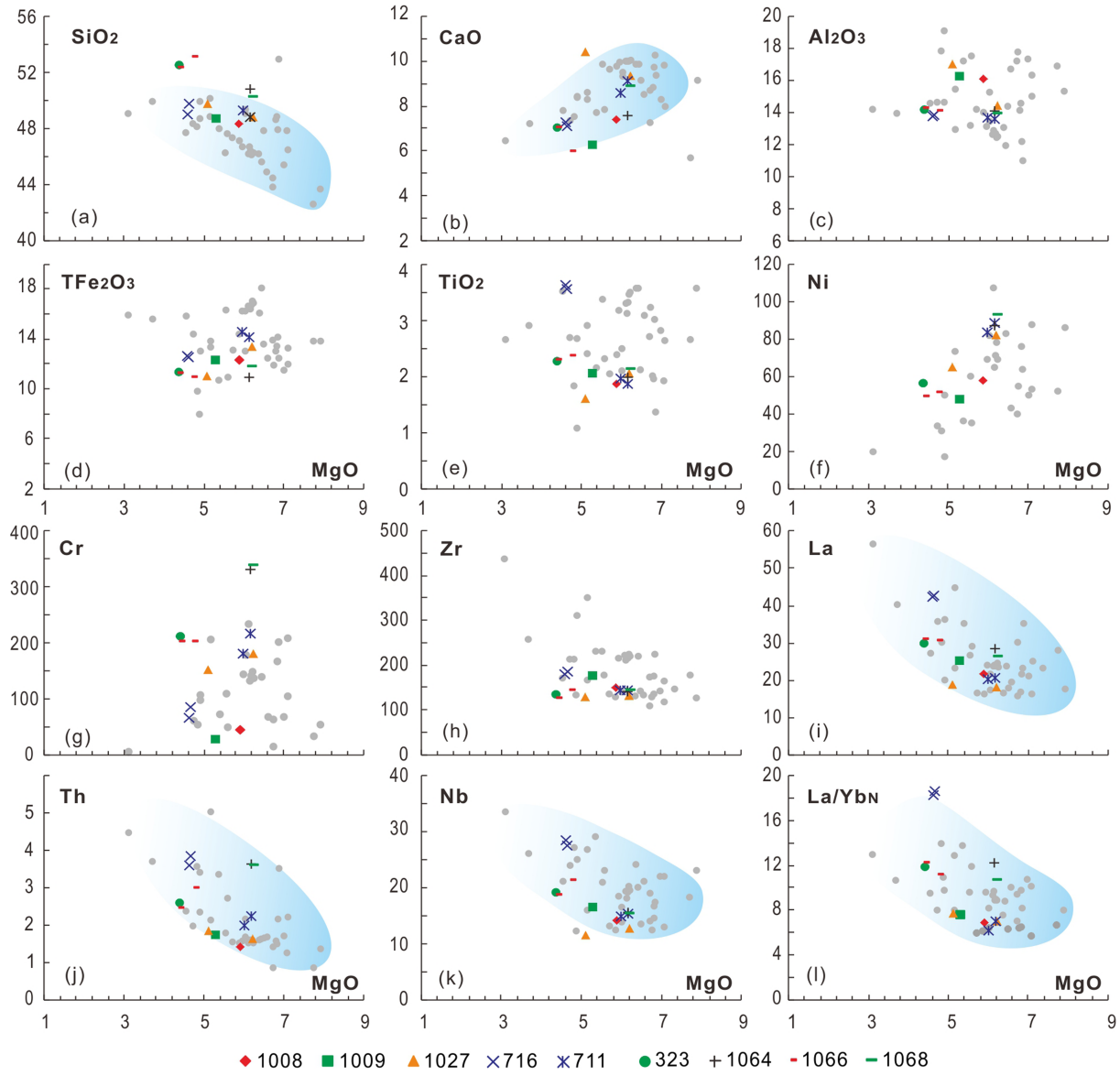

Figure 5. Major and trace elements (ratios) covariant plots. Gray dots are the same as those in Figure 4. Blue fields show broad data trends.

5.3. Rock Magnetic and Magnetic Fabric Results

All the samples have an unblocking temperature of ~580 °C (the Curie temperature of magnetite) and show Hopkinson peaks (Dunlop & Özdemir, 1997) in thermomagnetic curves (Figure 7), indicating the presence of highly paleomagnetically stable single-domain (SD) or pseudo-single-domain (PSD) low-Ti titanomagnetite or pure magnetite. Many representative samples also show nearly reversible heating and cooling curves (Figures 7c and 7e–7j), confirming that little mineralogical changes occurred at high temperatures. A minor presence of pyrrhotite can explain the increases in magnetic susceptibility of heating curves around 200–300 °C and the decreases around 300–400 °C in some samples (Figures 7b and 7d).

The triaxial thermal demagnetization of IRM analyses demonstrated a domination of soft magnetic components, with unblocking temperature of 550–600 °C (~520 °C for sample 517-4-1), implying the occurrence of Ti-poor multidomain (MD) titanomagnetite in many samples (Figure 8). However, in some cases, the paleomagnetically stable SD or PSD magnetite (intermediate components, 0.12–0.4 T) is also present (e.g., Figures 8a–8g).

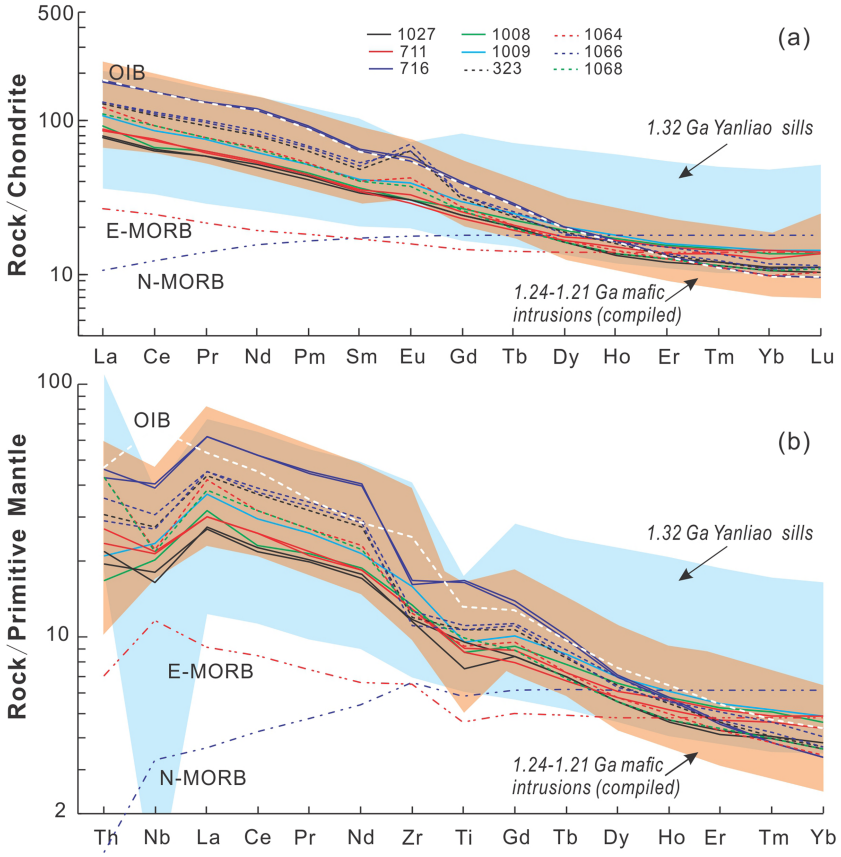

Figure 6. Chondrite-normalized REE patterns (a) and primitive mantle-normalized multielement spidergrams (b). OIB, E-MORB, N-MORB, chondrite normalized values, and primitive mantle values are from Sun and McDonough (1989). The complied data for the 1.24–1.21 Ga mafic intrusions as in Figure 4. The data for the 1.32 Ga Yanliao LIP ($N = 45$) in the NCC are from Zhang et al. (2017).

Both magnetic anisotropy parameters P and Pj are less than 1.10 (Figure S1). Dykes C711 shows more positive T values (AMS ellipsoid parameter) indicating a dominant oblate fabric; JD1027 shows more negative T values indicating a dominant prolate fabric (Figure S1) (Tarling & Hrouda, 1993). Moreover, these two dykes show normal magnetic fabrics (K_1–K_2 planes parallel to the dyke trends; Figure S1).

5.4. Paleomagnetic Results

5.4.1. 1.24 Ga Dykes

Dyke JD687 is regarded as a coeval dyke as the dated dykes JD517 and JD1027 (both at ~1,235 Ma; Figure 1d) according to their similar geochemical features (Wang et al., 2016), which is further verified by their similar paleomagnetic directions. Similar paleomagnetic directions also have been found in dykes C711, C716, LX323, LX1064, LX1066, and LX1068 (Figures 9 and 10; Table 2). This E-SE moderate to shallow downward stable characteristic remanence magnetization (ChRM) has been isolated after both thermal and AF demagnetization. Its unblocking temperature is close to ~580 °C, indicating magnetite as the remanence carrier (Figures 9a–9f). No antipodal directions have been found (Figures 9 and 10). Based on the similarity of remanence directions, we regard all these dykes belonging to the ~1.24 Ga group. In support to this suggestion, we note that closely located dykes C711 and C716 have similar trends and mineralogical characteristics (Figures 1c and 2j and 2k).

ChRM directions of nine 1.24 Ga dykes are shown in Table 2. The mean paleomagnetic pole for this group of dykes is at 2.0°N, 165.1°E ($A_{95} = 11.0°$). Seven out of nine dykes of this group (except LX323 and C716) also yield low temperature components (LTC) (Figure S2; Table S4). Most LTCs, being acquired below 280–310 °C

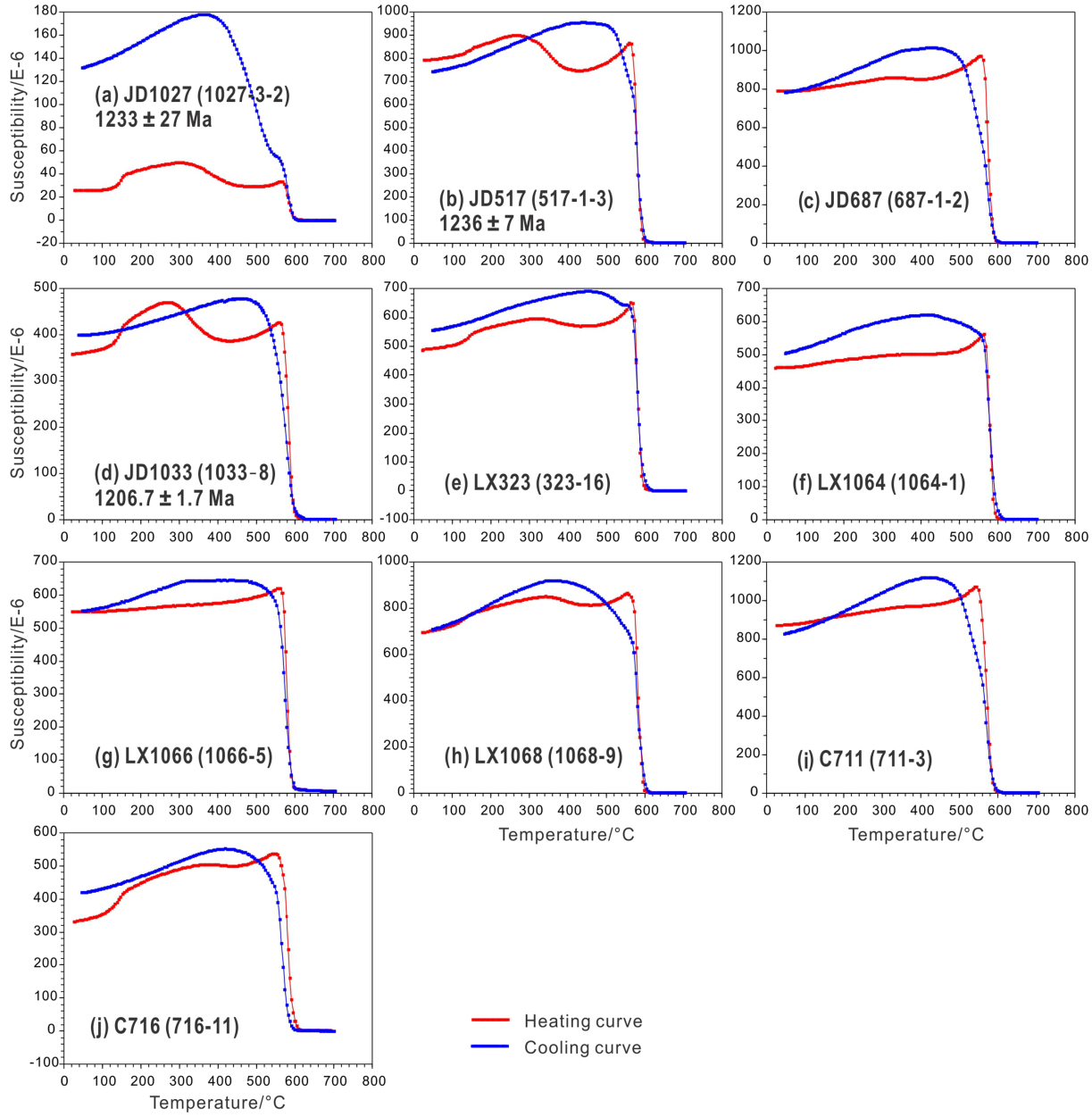

Figure 7. Result of susceptibility versus temperature (κ-T) of representative samples. Age details are in Table 1.

(Figure 9), are close to the directions of the present geomagnetic field (PGF) and geocentric axial dipole (GAD) (Figure S2).

Baked contact tests have been performed on dykes JD1027 and JD687 (Figure 1d), where country rocks are Archean gneisses. JD1027 is a ~30 m wide dyke, and we collected host rock samples adjacent to it within ~3 m and at >100 m from the dyke's margin. These gneisses are paleomagnetically stable, yielding moderate southeast downward ChRM direction near the dyke and moderate southwest upward direction at >100 m from the dyke (Figure 11a). This result illustrates that the host rocks adjacent to the dyke were reheated and remagnetized during the emplacement of the dyke; however, the host rocks far from the dyke were not affected by the dykes. We interpret this as a positive contact test and consider the ChRM as primary.

For the ~25 m wide JD687 dyke, we collected country rocks within ~35 cm and at >35 m from the dyke. The adjacent host rocks also show stable remanence direction similar to the dyke's direction. Although the

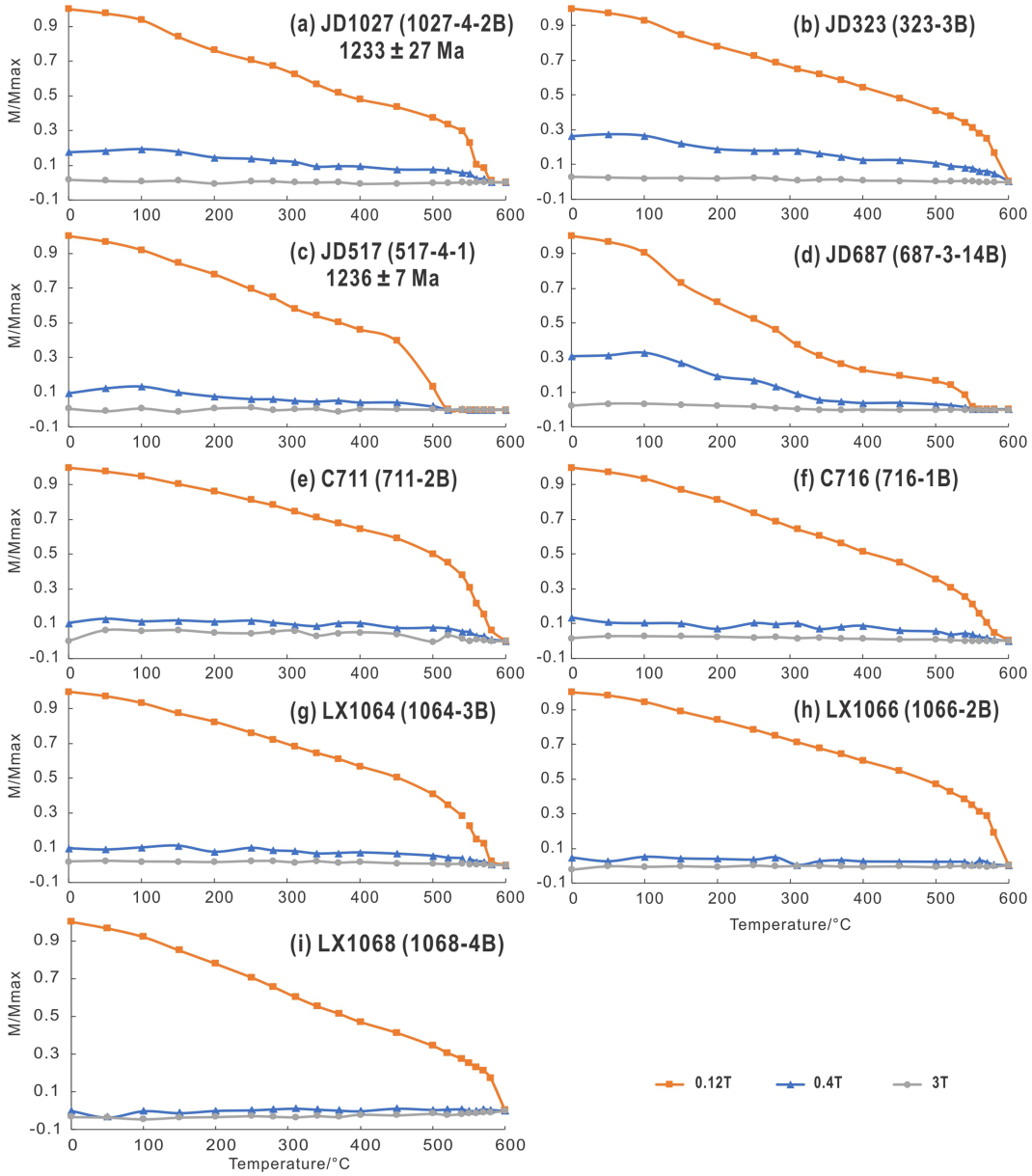

Figure 8. Triaxial isothermal remanent magnetization (IRM) of representative samples. Age details are in Table 1.

unbaked host rocks yield scattered ChRM directions (Figure 11b), they are nonetheless different from the dyke's direction, suggesting a positive (though weaker) test result.

5.4.2. 1.21 Ga Dyke

The 1,206.7 ± 1.7 Ma dyke MY1033 locates in the Miyun county (Figure 1d). This dyke is about 30 Ma younger than the other studied dykes (Table 1) and gives a different remanent direction: SW moderate downward (Figure 10j; Table 2). Both thermal (Figure 9g) and AF (Figure 9h) demagnetization isolated a stable ChRM with 540–580 °C unblocking temperatures and >40 mT coercivity. The mean paleomagnetic direction is D = 204.5°, I = 39.5°, α_{95} = 6.5°, and the corresponding paleopole is 23.0°S, 92.5°E, dp/dm = 4.7°/7.8°. This pole should be considered a virtual geomagnetic pole (VGP) because it is based on the paleomagnetic direction from just one dyke that does not average out secular variations. The LTC direction, mostly being acquired below 520 °C, is D = 1.3°, I = 73.3°, α_{95} = 8.9°, which is close to the PGF and GAD directions (Figure S2h; Table S4).

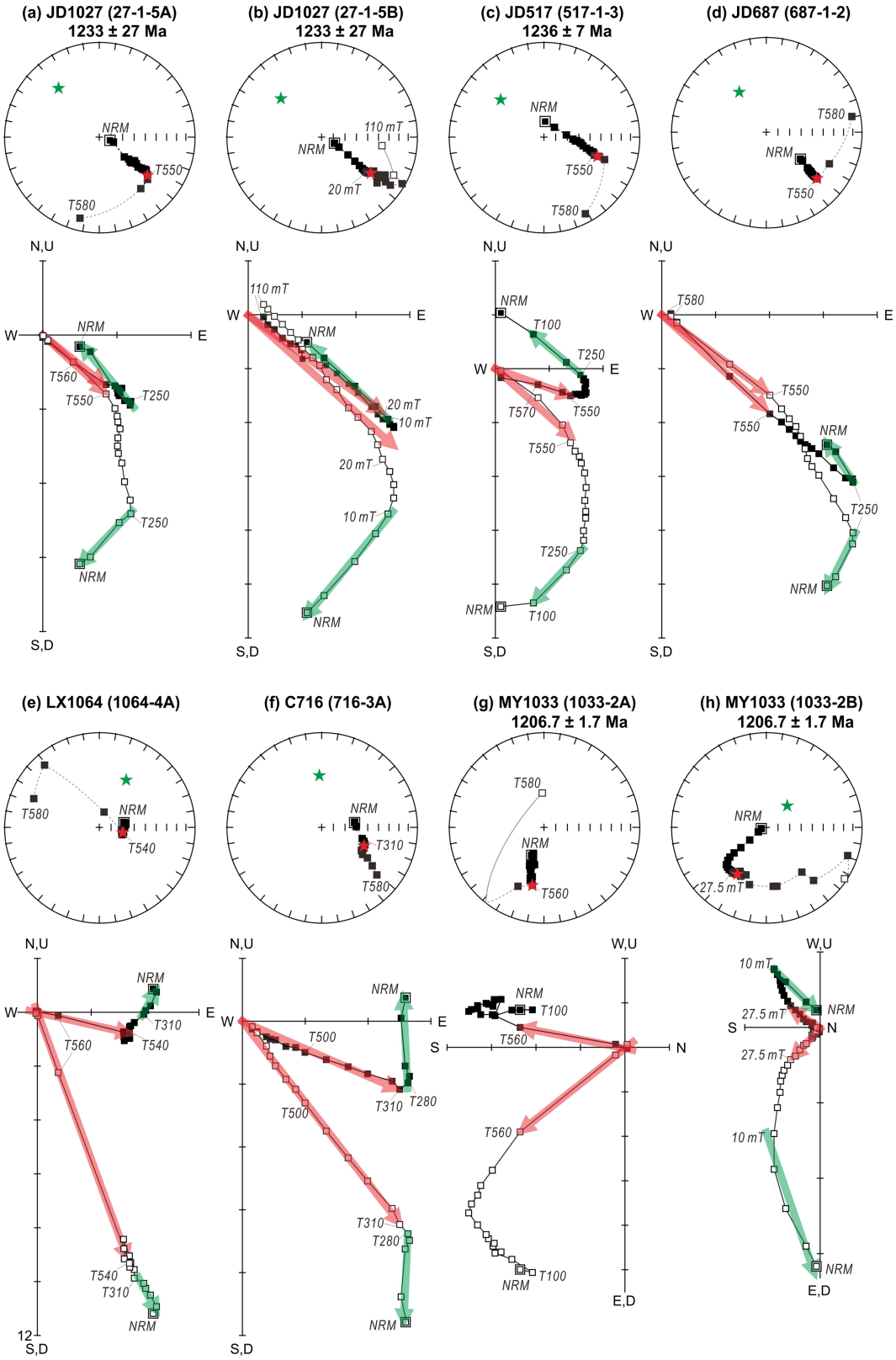

Figure 9. Thermal and AF demagnetizations of the 1.24 Ga (a–f) and the 1.21 Ga (g–h) dykes: Equal area stereoplots (solid/open square points correspond for downward/upward-pointing magnetizations; green/red stars represent vector directions of low/high temperature components) and orthogonal projection diagrams (solid/open square points show vector end points projections onto the horizontal/vertical plane).

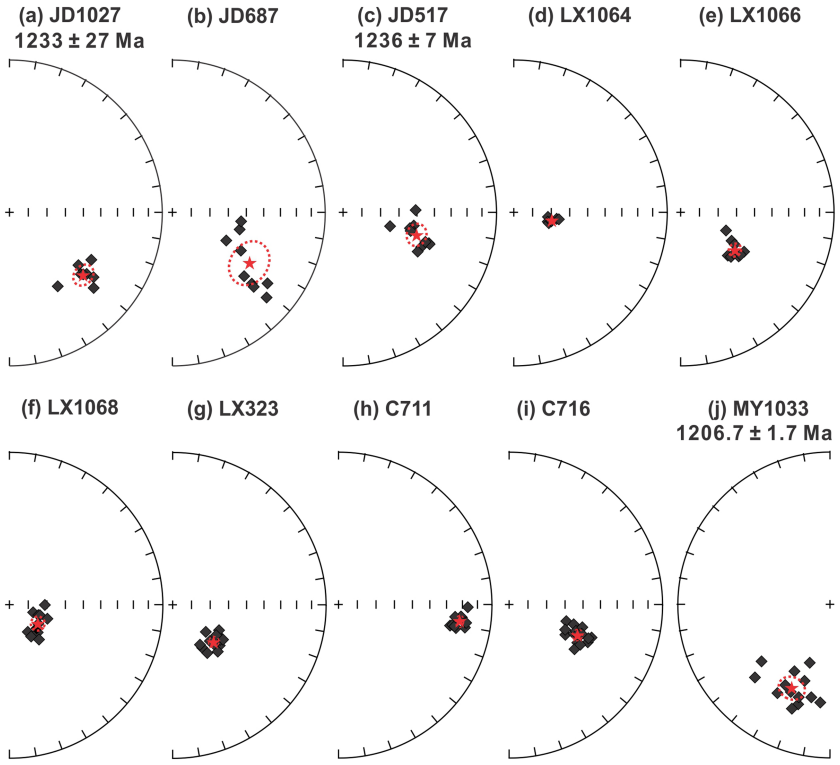

Figure 10. Equal-area projections showing the ChRM of each dyke. Each diamond represents one sample. Red stars and surround dashed line represent the site/dyke mean directions and α_{95} ovals. Solid symbols represent lower hemisphere vectors.

6. Discussion

6.1. Petrogenesis of the 1.24–1.21 Ga Dykes

The reported late Mesoproterozoic rock units and geochronological results in the NCC are listed in Table 1. These units mainly consist of mafic dykes, showing U–Pb ages of 1,244–1,207 Ma. We consider this as a

Table 2
High Temperature Component Results of Paleomagnetic Sites

Dyke ID (age/Ma)	Width (m)	Trend (°)	Lat (°N)	Long (°E)	n/N	Dec (°)	Inc (°)	α_{95} (°)	Plat (°N)	Plong (°E)	dp/dm (°)
JD517 (1,236 ± 7)	>15	~34	39.857	118.920	10/13	107.0	48.3	5.6	6.8	176.0	4.8/7.3
JD687	~25	~4	40.261	118.482	9/12	123.5	39.3	11.1	−8.3	169.8	7.9/13.3
JD1027 (1,233 ± 27)	30–40	~24	40.245	118.486	8/12	130.3	36.6	5.4	−13.8	165.9	3.7/6.3
C711	>15	~310	37.400	114.187	11/11	98.0	21.0	2.7	0.4	190.7	1.5/2.8
C716	>15	~310	37.574	114.304	15/15	114.0	49.4	2.9	1.7	166.4	2.6/3.8
LX323	~15	~345	35.396	118.181	13/15	132.1	60.3	2.8	−1.6	152.1	3.2/4.3
LX1064	10	~350	35.872	118.120	7/15	101.9	69.3	1.9	21.5	157.5	2.8/3.3
LX1066	~20	~352	35.350	118.193	10/11	124.8	54.4	3.4	−2.9	160.6	3.3/4.7
LX1068	~15	~352	35.341	118.181	11/11	123.7	71.8	3.7	13.6	146.2	5.7/6.5
					9 site-level mean				2.0	165.1	A_{95} = 11.0°
MY1033 (1,206.7 ± 1.7)	~80	~35	40.617	117.083	13/13	204.5	39.5	6.5	−23.0	92.5	4.7/7.8
Dyke JD1027 baked contact test											
JD1027 (1,233 ± 27)	Baked host rocks ~3 m				8/8	127.3	27.7	7.6			
	Unbaked host rocks >100 m				5/8	215.5	−54.1	10.8			
Dyke JD687 baked contact test											
JD687	Baked host rocks ~0.35 m				5/6	118.7	52.6	15.0			
	Unbaked host rocks >35 m				6/9	79.4	−43.9	21.3			

Note. Lat (latitude) and Long (longitude) are sampling GPS locations; n/N, number of samples used/measured; Dec, declination; Inc, inclination; α_{95} and A_{95} are 95% radii confidence circles for direction and poles; dp and dm are semi-axes of elliptical error around the pole at a probability of 95%; Plat and Plong are latitudes and longitudes of paleopoles.

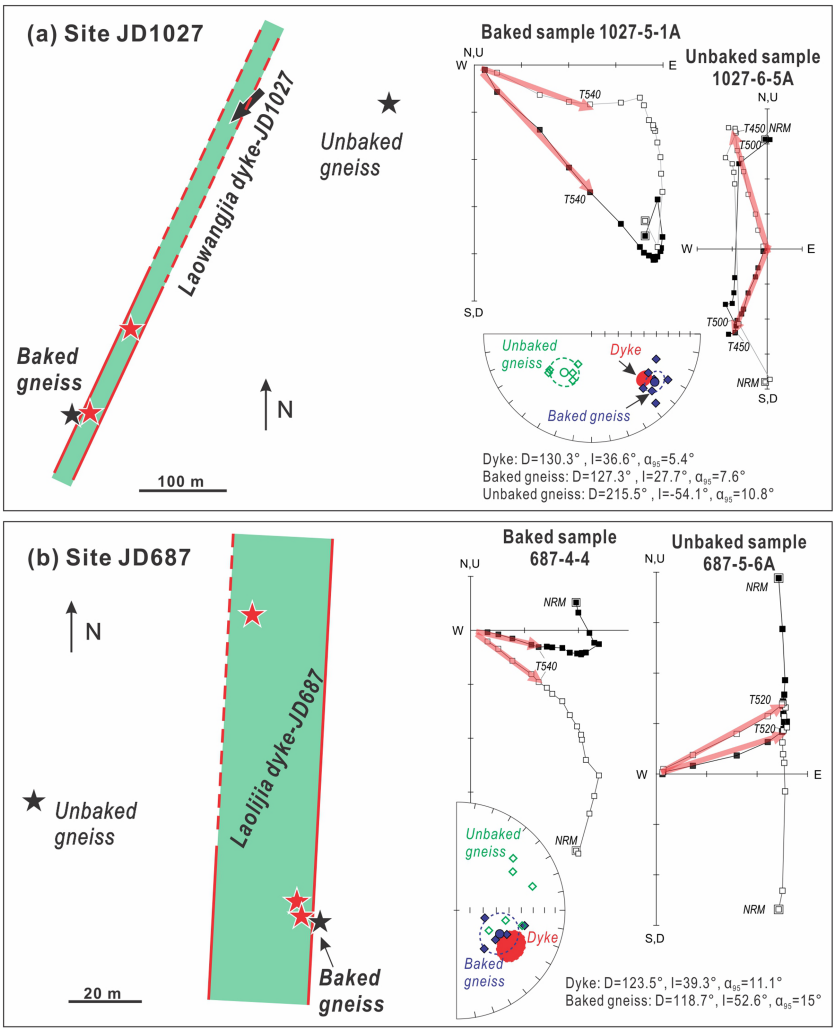

Figure 11. Baked contact tests for dykes JD1027 (a) and JD687 (b). Schematic diagrams include the margins of dykes (red solid lines; dashed lines are putative margins), sampling locations (stars), representative demagnetization of host gneisses (solid/open square points show vector end points projections onto the horizontal/vertical plane), and site-mean plots (solid/open square points correspond for downward/upward-pointing magnetizations).

single magmatic event in the NCC based on overlapping age ranges and similarities in geochemical characteristics (Figures 4–6). Geochemical data used for petrogenetic analyses include those from the dated units (Table S5) and nine other individual dykes (Table S3). Note that the geochemical data of the Baihejian dyke (MY1033) and Licheng dyke are in Peng et al. (2012) (sample 07MY12) and Peng, Bleeker, et al. (2011) (sample 05LC06), respectively (Table S5).

To estimate the geochemical effect of the observed alteration on bulk rock chemical composition, we compared the LOI with major and trace elements (Figure S3). Most elements show no correlation with LOI. However, some elements such as Al, Ca, and Rb displayed weak linear correlation with LOI, reflecting mobilization of these elements during the (plagioclase) alteration process (Figures 2g–2l) (see thin sections in Peng et al., 2013; C. Wang et al., 2016; W. Wang et al., 2015). In addition, Zr is generally considered as the most immobile element during alteration (e.g., Polat et al., 2002). Zr shows a positive linear correlation with high field strength elements (HFSEs: Nb, Ta, Hf, Th, REE [La, Sm, and Yb] and U), and no correlation with large-ion lithophile elements (LILEs: Rb, Sr, and Ba) (Figure S4). Thus, the HFSEs and REEs are considered more reliable in deciphering the petrogenesis of the studied rocks than LILEs.

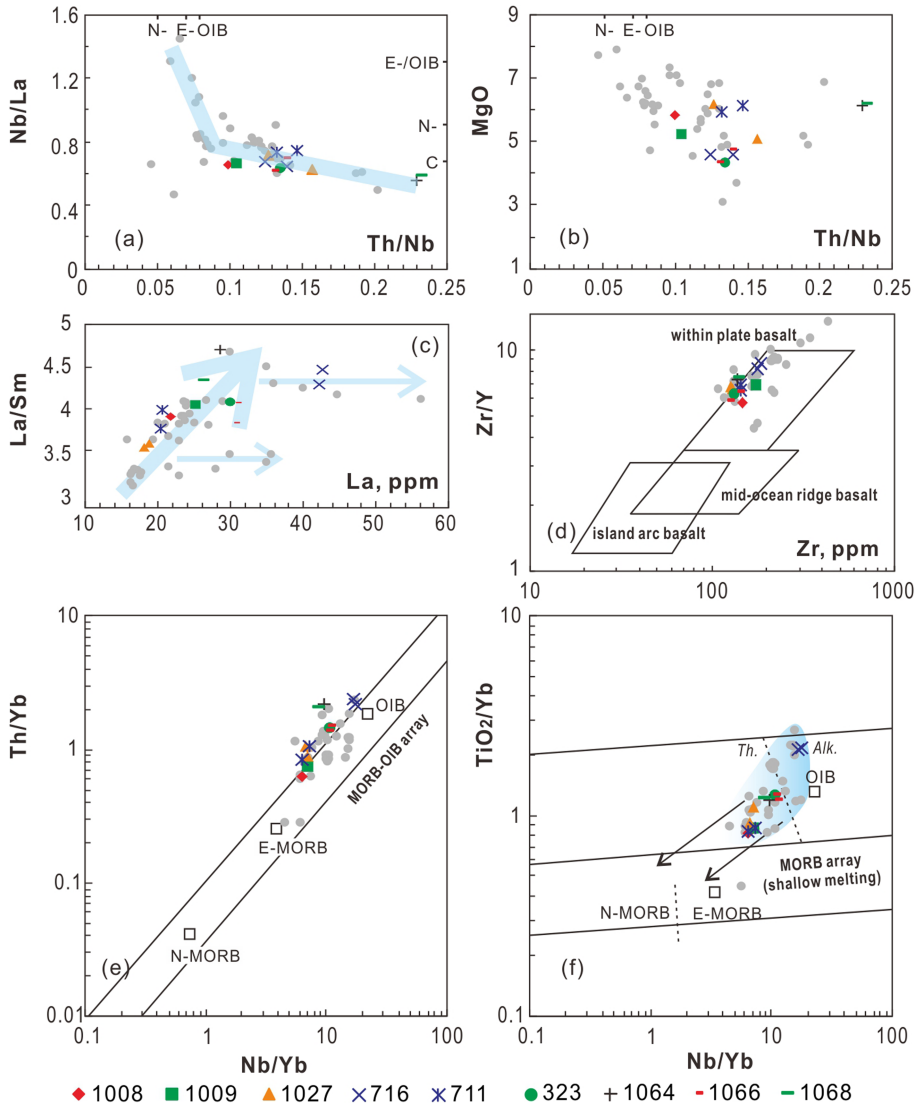

Figure 12. Trace elements ratio diagrams of the 1.24–1.21 Ga dykes. Gray dots are compiled data (Table S5).

Mafic intrusions can be contaminated by the host crustal rocks during emplacement. Some trace elements (e.g., Nb, La, and Th) and their ratios are sensitive to this process because of their distinct differentiation between crust and mantle (e.g., Pearce, 2008). The Nb/La ratios of N-MORB, E-MORB, OIB, and average crust are 0.93, 1.32, 1.30, and 0.67, while the Th/Nb ratios are 0.05, 0.07, 0.08, and 0.48, respectively (Sun & McDonough, 1989; Taylor, 1964). Some samples of this magmatism present low Th/Nb ratios (~0.05 to 0.09) and high Nb/La ratios (~0.8 to 1.3), indicating a low degree of crustal contamination (Figure 12a). These samples are mainly from the Jianping dyke (Figure 1d), which contain few inherited zircons (Wang et al., 2015), further supporting little crustal contamination during emplacement. However, some samples show relatively high Th/Nb, such as ratios of ~0.13–0.16 from JD1027 dyke and of ~0.23 from LX1064 and LX1068 dykes (Figure 12a), indicating a somewhat higher degree of crustal contamination. Also, zircon xenocrysts were found in the Laowangjia dyke (JD1027; not shown), supporting this conclusion. All these suggest nonhomogeneous crustal contamination among these dykes.

Multiple geochemical proxies, especially the continuous variations in elements (Figures 4 and 5), parallel REE, and spider patterns (Figure 6), indicate that these dykes likely shared the same source even if the event lasted for about 30 Ma. None of the studied samples were derived from primary magma since all Mg# values are <60 (Tables S3 and S5) (Frey et al., 1978). There is no obvious correlation between MgO and Al_2O_3,

tFe_2O_3, TiO_2, Cr, and Ni (Figures 5c–5g), so fractional crystallization seems to be a minor influence, which is also supported by the La/Sm versus La diagram (Figure 12c). In early magmatic evolution, the magma mainly experienced partial melting showing oblique linear tendency between La/Sm and La (Figure 12c). It gave way to weak crystallization-influenced differentiation when La reached a level over ~30 ppm (Figure 12c). Some samples show a weakly to significantly positive Eu-anomaly (Figure 6a), reflecting only a minor influence of plagioclase extraction.

Ratios of La/Yb_N generally range from 6.8 to 13.9, with values up to 18.6 (Figure 5l; Tables S3 and S5), reflecting the variation of degree of partial melting. The highest La/Yb_N samples are from the C716 dyke in the central NCC, which display alkaline features (Figure 4), but the C716 dyke shows no other extraordinary geochemical features compared with other dykes, besides showing more depleted HREE (Figures 5 and 6). All the samples have high REE contents (96–308 ppm), high La/Yb_N (6.8–18.6), which distinguish them from MORB. The Th-Nb proxy indicates an OIB affinity but with slight interaction with E-MORB (Figure 12e). Their high TiO_2/Yb ratios (Figure 12f) are indicative of garnet residues, and the rocks likely originated from melting beneath a thick lithosphere (Pearce, 2008). The diagonal trends from the OIB to the MORB fields reflect hot mantle flows within the lithosphere (Figures 12e–12f) (Pearce, 2008). Some samples show εHf (t = 1230 Ma) of 1.8–10 (Wang et al., 2015) and εNd (t = 1230 Ma) of 0–1.6 (Peng et al., 2013; Wang et al., 2016), which is suggestive of their originating from a depleted asthenosphere. Additionally, these dykes have high Ti content (usually >1.5 wt.%), indicating possibly a similar plume-related source as the Emeishan flood basalts (Xu et al., 2001).

6.2. Characteristics of the 1.24–1.21 Ga LIP Event in the NCC

A LIP-generating event refers to mantle plume-induced, high-volume magmatic activity during a period of up to tens of million years, which are sometimes associated with continental breakup (Ernst, 2014). A LIP event can be characterized by its volume (>0.1 Mkm^3), area (>0.1 Mkm^2), and duration (<50 Ma) and commonly represents a pulsed sequence of magmatism in an intraplate tectonic setting (Ernst, 2014 and references therein). Several of these characteristics are identifiable from the 1.24–1.21 Ga magmatism in the NCC.

First is the areal extent. The studied dykes are discontinuous in the field, and each can only be traced over several hundred meters, or a few kilometers, making it difficult to evaluate the total areal extent and volume. These dykes are in general over 10 m in width but can be up to 80 m wide, a scale commonly associated with LIPs (Ernst, 2014). After restoring the effect of the Tan-Lu fault (a sinistral strike-slip fault in the Phanerozoic; Zhao et al., 2016), this event is estimated to cover an area of $>0.1 \times 10^6$ km^2 in the central and eastern NCC (Figure 1). If the small dykes in the Bayan Obo rift (1227 ± 60 Ma, Sm-Nd isochron; Yang et al., 2011) are included, and if the PS dykes (Figure 1c) also belong to the same generation (Ding, 2017), the areal extent is even larger.

Second is the age spread. Constrained by the age data, this magmatic event lasted from ca. 1,244 to 1,207 Ma (U–Pb ages), with a total duration of ~30 Ma (Table 1). Considering the age uncertainties, and their consistent geochemical characteristics (Figures 4–6), we regard these dykes as belonging to the same LIP event. Ernst (2014) concluded that LIPs with >20 Ma age span were emplaced in several shorter duration pulses rather than as a single continuous episode. The resolution of our ages and limited sampling precludes a confident identification of discrete pulses of dyke emplacement; the three age populations, however—~1,230, ~1,220, and ~1,207–1,210 Ma (Table 1)—suggests multiple pules of magmatism.

Third is an intraplate origin. These intrusions were emplaced within the NCC and have intraplate geochemical characteristics (Figure 12d). Moreover, this dyke swarm present a fan-like radiating geometry in the field (Figure 1). Considering all, we interpret that the studied rocks originated from a mantle plume source.

Magnetic anisotropy has been widely used to estimate the directions of magma flows (e.g., Ernst & Baragar, 1992). The normal magnetic fabric of dyke JD1027 presents by the K_1 axis with shallow inclination (Figure S1a; Table S6), indicating the magma flowed laterally in this region far from the source. Conversely, the C711 dyke might have been emplaced closer to the magmatic centre since K_1 axis yields medium to steep inclinations (Figure S1b; Table S6). The geometry of the dykes and their magnetic fabrics suggest that the magmatic center could be in the southeastern NCC, possibly around the Luxi area (Figure 13b). We suggest

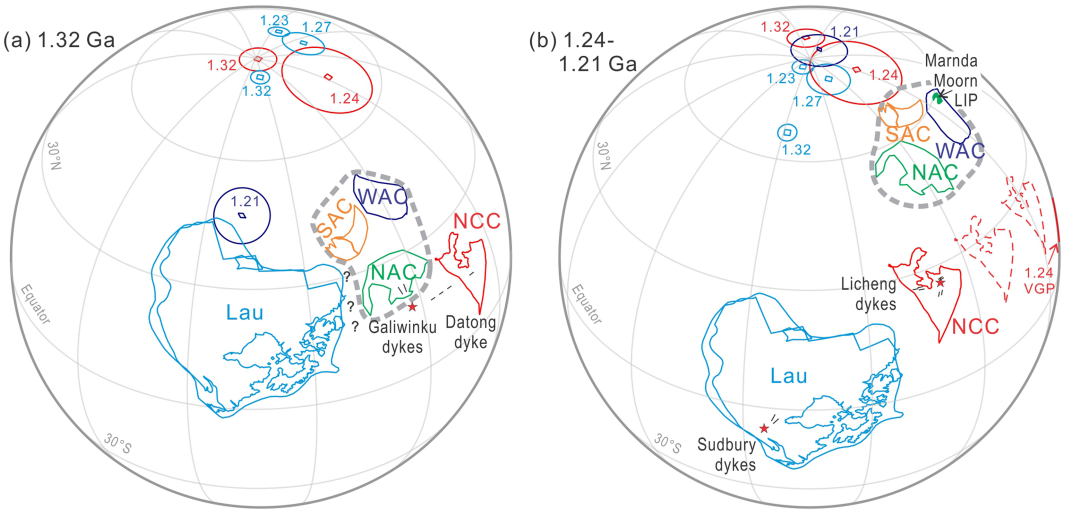

Figure 13. Paleogeographic reconstruction among the NCC, proto-Australia, and Laurentia (Lau) at 1.32 Ga (a) and 1.24–1.21 Ga (b). The paleopoles are marked with ages in Ga. Red star represents interpreted location of the mantle plume. The proto-Australia configuration is after Li and Evans (2010), where the South and West Australian cratons (SAC and WAC) had an ~40°clockwise rotation relative to the NAC in Neoproterozoic. Euler rotation parameters for 1.32 Ga (a): NCC (−32.72°N, −44.19°E, −124.58) and NAC (−4.44°N, −55.92°E, −178.78) after Wang et al. (2019), Lau (35.86°N, 156.02°E, 112.21); for 1.24–1.21 Ga (b): NCC (−28.86°N, −61.71°E, −104.44), NAC (14.03°N, 110.22°E, 133.23), Lau (35.24°N, 149.25°E, 127.30).

that the dyke swarms collectively form a 1.24–1.21 Ga LIP related to a plume event in the NCC, which is named as the Licheng LIP (after the 1.23 Ga Licheng dyke swarm first identified by Peng (2015)).

6.3. Implications for Paleogeographic Reconstruction

Dyke LX1064 was dated at 1,841 ± 17 Ma through the zircon U–Pb LA-ICPMS method (Wang et al., 2007), though the exact nature of dated zircons is difficult to definitively determine through examination of a few unclear zircon CL images. It cannot be ruled out that these are inherited zircons. This generation of magmatism in the NCC has not been confirmed by more recent studies (Peng, 2015 and references therein). Considering that this dyke has a similar magnetic direction as those from ~1.24 Ga dykes, we suggest that it should be part of the ~1.24 Ga magmatism. With this assumption, our results from a total of nine dykes yield a mean paleomagnetic pole at 2.0°N, 165.1°E, A_{95} = 11.0° (Table 2) with a positive baked contact test (Figure 11). It thus represents a primary key paleopole for the NCC. The slightly younger 1,206.7 ± 1.7 Ma Baihejian dyke (MY1033) yields a different ChRM direction (Figure 10j; Table 2) and provides a ~1.21 Ga VGP.

Selected paleomagnetic poles are listed in Table 3 for assessing regional paleogeography. Here, we discuss the reconstruction and relationships among the NCC, proto-Australia, and Laurentia from ~1.4 to ~1.2 Ga. First, a long-lasting connection between the NCC and the NAC in the Mesoproterozoic has been proposed based on the similarity between their APWPs and their comparable tectonostratigraphic records, including coeval magmatism, ore deposits, fossils, and comparable hydrocarbon-bearing potential layers (Wang et al., 2019). Paleomagnetic reconstruction based on the updated 1.24 Ga paleomagnetic poles indicates that the two continents likely have started to pull away from each other, or at least the connection of northeastern NCC and northern NAC has been broken by that time (Figure 13). This is consistent with the previous suggestion of a breakup of the NCC from the NAC at ca. 1.32 Ga based on the presence of unconformities within the NCC (between the Xiamaling Formation and the overlying Changlongshan Formation) and the NAC (between the Roper Group and the overlying Cambrian volcanics) (Ahmad et al., 2013; Zhang et al., 2017). Considering that the likely plume-triggered 1.32 Ga mafic magmatism occurred after the deposition of the Xiamaling Formation and the Roper Group, the two unconformities might represent the breakup event or plume-related uplift and erosion (Zhang et al., 2017). We notice that

Table 3
Selected Paleopoles for Paleogeographic Reconstruction

Rock unit	Age (Ma)	Age reference	Plat (°N)	Plong (°E)	A_{95} (°)	Quality criteria[a]	Reference
North China Craton							
Yanliao mafic sills (Yanliao LIP)	1,330–1,300	Zhang et al., 2017	5.9	359.6	4.3	+ + + + + − +	Chen et al., 2013
Licheng-Maojiagou dykes (Licheng LIP)	1,236 ± 7; 1,233 ± 27	Wang et al., 2016; This study	2.0	165.1	11.0	+ + + + + − +	This study
Baihejian dyke-VGP	1,206.7 ± 1.7	This study	−23.0	92.5	6.1	+ − + − + − +	This study
Western Australian Craton							
Gnowangerup–Fraser dyke swarm (Marnda Moorn LIP)	1,218 ± 6; 1,211 ± 42; 1,218–1,202; ca. 1,210	Pisarevsky, Wingate, et al., 2014 and references therein	−55.8	143.9	6.5	+ + + + + + −	Pisarevsky, Wingate, et al., 2014
Laurentia							
Nain anorthosite	1,322 ± 1; 1,320–1,290	Hamilton et al., 1998 and references therein	11.7	206.7	2.2	+ + + − − + +	Murthy, 1978
Mackenzie dykes (Mackenzie LIP)	1,267 ± 2	LeCheminant & Heaman, 1989	4.0	190.0	5.0	+ + + + + − +	Buchan & Halls, 1990;
Sudbury dykes	1,235 + 7/− 3	Dudas et al., 1994	−2.5	192.8	2.5	+ + + + + − +	Palmer et al., 1977

[a]Quality criteria from left to right are (1) well-determined rock age, (2) sufficient samples ($N > 24$, $k \geq 10$, $A_{95} \leq 16.0°$), (3) step-wise demagnetization, (4) field tests, (5) structural control and tectonic coherence with the craton discussed, (6) presence of reversals, and (7) no resemblance to paleopoles of younger age (Van der Voo, 1990). "+" indicates a criterion is met; otherwise, it is marked as "−".

the Licheng LIP of NCC may potentially be linked to the Marnda Moorn LIP of the West Australian Craton (WAC) (Ernst et al., 2008) at 1.24–1.21 Ga (dotted optional position for the NCC in Figure 13b).

Second, the Georgetown Inlier of northeast Australia is thought to be linked to northwest Laurentia in the early Mesoproterozoic according to detrital zircon spectra and metamorphism analyses (Nordsvan et al., 2018; Pourteau et al., 2018). However, this configuration may have been somewhat modified by at ~1.32 Ga based on our reassessment using ~1.32 Ga poles, featuring a clockwise rotation of proto-Australia relative to Laurentia (Figure 13a). If so, the rifting between Laurentia and proto-Australia would have occurred before then, possibly represented by the 1.39–1.38 Ga Salmon River arch mafic rocks and Hart River sills of the western Laurentia (Verbaas et al., 2018) and the Biberkine dyke swarm of the Yilgarn Craton (Stark et al., 2018).

Third, the Sudbury dykes of Laurentia are located along the eastern margins of Laurentia (Figure 13b); both these dykes and the Licheng dykes were emplaced at ~1.23 Ga, interpreted as large igneous events (Ernst & Bleeker, 2010; Ernst et al., 2008 and this study). Our paleomagnetic reconstruction implies that the two swarms had to be independent magmatic events as the NCC and Laurentia were not connected at that time (Figure 13b).

In summary, our paleogeographic reconstruction for 1.24–1.21 Ga implies a dispersed Laurentia, NCC, and proto-Australia, indicating that the component cratons of the Nuna supercontinent were separated from each other by that time.

Wang et al. (2015) suggested that the 1.24–1.21 Ga magmatism in NCC with the ~1.27–1.21 Ga magmatism in Laurentia, Baltica, and São Francisco cratons has been caused by a single mantle plume. Such an interpretation requires these blocks to drift over the same mantle plume, each traveling a long distance over ~60 Ma. One possible tectonic explanation for the Licheng LIP is that this event could be a late-stage activity of the same mantle plume responsible for the 1.32 Ga Yanliao LIP in the northern NCC. After separating NAC and NCC at 1.32 Ga, the two cratons drifted separately, and the NCC moved over the relatively stationary plume head at ca. 1.24 Ga (Figure 13). The 1.32 and 1.24–1.21 Ga magmatic rocks of the NCC indeed show similar εNdt values (0–2; Peng et al., 2013; Wang et al., 2016; Zhang, Zhao, et al., 2012), raising the possibility of associated source(s). Their different REE and spider patterns (Figure 6) could be due to differences in melting depth and/or varying influence of residual garnet.

7. Conclusions

A combination of field investigation with geochronological and geochemical studies allowed us to define a $>0.1 \times 10^6$ km^2 Licheng LIP in the NCC. This intraplate magmatic event continued for at least ~1,244 to ~1,207 Ma. The studied mafic dykes have OIB-like features in trace-element ratios and patterns and show radial geometry, indicating a plume origin. Rock magnetic studies show the dykes have stable magnetizations carried by SD or PSD magnetite. Nine dykes yield a ~1.24 Ga paleomagnetic pole at 2.0°N, 165.1°E, A_{95} = 11.0°, supported by positive baked contact test. The paleomagnetic analyses show that the NCC separated from proto-Australia after 1.32 Ga and remained unconnected to Laurentia, indicating the breakup of the supercontinent Nuna occurred by this time. Using the reconstructed drift history of the NCC and comparable geochemical characteristics between the 1.24–1.21 Ga and the 1.32 Ga mafic rocks, we suggest that the NCC may have twice sampled a relatively stationary mantle plume at 1.32 and 1.24–1.21 Ga, respectively.

Acknowledgments
The first author thanks Ross Mitchell, Uwe Kirscher, Josh Beardmore, and Lei Wu for their help in paleomagnetic studies and thanked Qian Zhao, Shuyan Yang, Fengbo Sun, Xiaotong Zhou, Zhiyue Zhang, Dongjian Ouyang, Guohua Cheng, and Hongyu Gu for their help in the field and experiments. We appreciate the reviews and comments from Profs. Richard Ernst and Michiel de Kock. Financial support for this study was provided by National Natural Science Foundation of China (NSFC) project (No. 41890833 and No. 41772192), the Advanced Science Key Research Project of Chinese Academy of Sciences (QYZDB-SSW-DQC04281712250), and Australian Research Council (ARC) Laureate Fellowship project (FL150100133). This is a contribution to International Geoscience Programme (IGCP) 648 and the Academy of Finland project 319277. Readers can freely access to the data of this paper from the Open Science Framework database (https://osf.io/j95g7/).

References

Ahmad, M., Dunster, J., & Munson, T. (2013). Chapter 15: McArthur Basin. In M. Ahmad & T. J. Munson (Eds.), *Geology and mineral resources of the Northern Territory*. *Special Publication* (Vol. 5, pp. 15:1–15:72). Darwin: Northern Territory Geological Survey.

Bleeker, W., & Ernst, R. (2006). Short-lived mantle generated magmatic events and their dyke swarms: The key unlocking Earth's paleogeographic record back to 2.6 Ga. In E. Hanski, S. Mertanen, T. Ramo, & J. Vuollo (Eds.), *Dyke swarms–time markers of crustal evolution* (pp. 3–26). London: Taylor & Francis Group.

Buchan, K., & Halls, H. (1990). Paleomagnetism of Proterozoic mafic dyke swarms of the Canadian shield. In *Mafic dykes emplacement mechanisms* (pp. 209–230). Rotterdam: Balkema.

Chen, L., Huang, B., Yi, Z., Zhao, J., & Yan, Y. (2013). Paleomagnetism of ca. 1.35Ga sills in northern North China Craton and implications for paleogeographic reconstruction of the Mesoproterozoic supercontinent. *Precambrian Research*, *228*, 36–47. https://doi.org/10.1016/j.precamres.2013.01.011

Ding, J. (2017). A combined Geochronological and Paleomagnetic study on ~1220 Ma mafic dykes in the North China Craton and its implications for the transition from Nuna to Rodinia. *(Doctoral dissertation)*. Beijing: China University of Geosciences (Beijing).

Dudas, F., Davidson, A., & Bethune, K. (1994). Age of the Sudbury diabase dykes and their metamorphism in the Grenville Province, Ontario. Radiogenic age and isotopic studies. *Current research, part F. Geological Survey of Canada, Report*, *8*, 97–106.

Dunlop, J. D., & Özdemir, Ö. (1997). In D. Edwards (Ed.), *Rock Magnetism: Fundamentals and frontiers* (pp. 1–573). Cambridge: Cambridge University Press.

Ernst, R., & Bleeker, W. (2010). Large igneous provinces (LIPs), giant dyke swarms, and mantle plumes: Significance for breakup events within Canada and adjacent regions from 2.5 Ga to the Present. *Canadian Journal of Earth Sciences*, *47*(5), 695–739. https://doi.org/10.1139/e10-025

Ernst, R., Head, J., Parfitt, E., Grosfils, E., & Wilson, L. (1995). Giant radiating dyke swarms on earth and Venus. *Earth-Science Reviews*, *39*(1–2), 1–58.

Ernst, R. E. (2014). *Large Igneous Provinces* (pp. 1–653). Cambridge: Cambridge University Press.

Ernst, R. E., & Baragar, W. R. A. (1992). Evidence from magnetic fabric for the flow pattern of magma in the Mackenzie giant radiating dyke swarm. *Nature*, *356*(6369), 511–513. https://doi.org/10.1038/356511a0

Ernst, R. E., Wingate, M. T. D., Buchan, K. L., & Li, Z. X. (2008). Global record of 1600–700Ma large igneous provinces (LIPs): Implications for the reconstruction of the proposed Nuna (Columbia) and Rodinia supercontinents. *Precambrian Research*, *160*(1–2), 159–178. https://doi.org/10.1016/j.precamres.2007.04.019

Evans, D., Li, Z.-X., & Murphy, J. (2016). Four-dimensional context of Earth's supercontinents. *Geological Society, London, Special Publications*, *424*, SP424.412.

Evans, D. A. D., & Mitchell, R. N. (2011). Assembly and breakup of the core of Paleoproterozoic-Mesoproterozoic supercontinent Nuna. *Geology*, *39*(5), 443–446. https://doi.org/10.1130/g31654.1

Frey, F. A., Green, D. H., & Roy, S. D. (1978). Integrated Models of Basalt Petrogenesis: A Study of Quartz Tholeiites to Olivine Melilitites from South Eastern Australia Utilizing Geochemical and Experimental Petrological Data. *Journal of Petrology*, *19*(3), 463–513. https://doi.org/10.1093/petrology/19.3.463%J

Furlanetto, F., Thorkelson, D. J., Daniel Gibson, H., Marshall, D. D., Rainbird, R. H., Davis, W. J., et al. (2013). Late Paleoproterozoic terrane accretion in northwestern Canada and the case for circum-Columbian orogenesis. *Precambrian Research*, *224*, 512–528. https://doi.org/10.1016/j.precamres.2012.10.010

Halls, H. C., Li, J., Davis, D., Hou, G., Zhang, B., & Qian, X. (2000). A precisely dated Proterozoic palaeomagnetic pole from the North China craton, and its relevance to palaeocontinental reconstruction. *Geophysical Journal International*, *143*(1), 185–203.

Hamilton, M., Ryan, A., Emslie, R., & Ermanovics, I. (1998). Identification of Paleoproterozoic anorthositic and monzonitic rocks in the vicinity of the Mesoproterozoic Nain plutonic suite, Labrador: U–Pb evidence, *Current research, part F. Geological Survey of Canada,* Paper, 23-40.

He, T., Zhou, Y., Vermeesch, P., Rittner, M., Miao, L., Zhu, M., et al. (2017). Measuring the 'great unconformity' on the North China Craton using new detrital zircon age data. *Geological Society, London, Special Publications*, *448*(1), 145–159. https://doi.org/10.1144/sp448.14

Heaman, L. M. (2009). The application of U–Pb geochronology to mafic, ultramafic and alkaline rocks: An evaluation of three mineral standards. *Chemical Geology*, *261*(1–2), 43–52. https://doi.org/10.1016/j.chemgeo.2008.10.021

Hou, G., Santosh, M., Qian, X., Lister, G. S., & Li, J. (2008). Configuration of the late Paleoproterozoic supercontinent Columbia: Insights from radiating mafic dyke swarms. *Gondwana Research*, *14*(3), 395–409. https://doi.org/10.1016/j.gr.2008.01.010

Jaffey, A., Flynn, K., Glendenin, L., Bentley, W., & Essling, A. (1971). Precision measurement of half-lives and specific activities of ^{235}U and ^{238}U. *Physical Review C*, *4*(5), 1889.

Kirscher, U., Liu, Y., Li, Z. X., Mitchell, R. N., Pisarevsky, S. A., Denyszyn, S., & Nordsvan, A. (2019). Paleomagnetism of the hart dolerite (Kimberley, Western Australia) - a two-stage assembly of the supercontinent Nuna? *Precambrian Research*, *329*, 170–181. https://doi.org/10.1016/j.precamres.2018.12.026

Kirschvink, J. (1980). The least-squares line and plane and the analysis of palaeomagnetic data. *Geophysical Journal of the Royal Astronomical Society*, *62*(3), 699–718.
Kusky, T., Li, J., & Santosh, M. (2007). The Paleoproterozoic North Hebei Orogen: North China craton's collisional suture with the Columbia supercontinent. *Gondwana Research*, *12*(1), 4–28. https://doi.org/10.1016/j.gr.2006.11.012
LeCheminant, A. N., & Heaman, L. M. (1989). Mackenzie igneous events, Canada: Middle Proterozoic hotspot magmatism associated with ocean opening. *Earth and Planetary Science Letters*, *96*(1), 38–48. https://doi.org/10.1016/0012-821X(89)90122-2
Li, Q.-L., Li, X.-H., Liu, Y., Tang, G.-Q., Yang, J.-H., & Zhu, W.-G. (2010). Precise U–Pb and Pb–Pb dating of Phanerozoic baddeleyite by SIMS with oxygen flooding technique. *Journal of Analytical Atomic Spectrometry*, *25*(7), 1107–1113.
Li, X. H., Liu, Y., Li, Q. L., Guo, C. H., & Chamberlain, K. R. (2009). Precise determination of Phanerozoic zircon Pb/Pb age by multi-collector SIMS without external standardization. *Geochemistry, Geophysics, Geosystems*, *10*, Q04010. https://doi.org/10.1029/2009GC002400
Li, Z. X., Bogdanova, S. V., Collins, A. S., Davidson, A., De Waele, B., Ernst, R. E., et al. (2008). Assembly, configuration, and break-up history of Rodinia: A synthesis. *Precambrian Research*, *160*(1–2), 179–210. https://doi.org/10.1016/j.precamres.2007.04.021
Li, Z. X., & Evans, D. A. D. (2010). Late Neoproterozoic 40 intraplate rotation within Australia allows for a tighter-fitting and longer-lasting Rodinia. *Geology*, *39*(1), 39–42. https://doi.org/10.1130/g31461.1
Liu, C., Zhao, G., Liu, F., & Shi, J. (2017). Detrital zircon U-Pb and Hf isotopic and whole-rock geochemical study of the Bayan Obo Group, northern margin of the North China Craton: Implications for Rodinia reconstruction. *Precambrian Research*, *303*, 372–391. https://doi.org/10.1016/j.precamres.2017.04.033
Lowrie, W. (1990). Identification of ferromagnetic minerals in a rock by coercivity and unblocking temperature properties. *Geophysical Research Letters*, *17*(2), 159–162.
Lu, S., & Li, H. (1991). A precise U-Pb single zircon age determination for the volcanics of Dahongyu Foramation, Changcheng system in Jixian. *Acta Geosicientia Sinica*, *22*(1), 137–145.
Ludwig, K. (2012). *Isoplot/ex, v. 3.75*, *Berkeley Geochronology Center Special Publication* (Vol. 5, pp. 1–75). Berkeley: Berkeley Geochronology Center.
Lurcock, P. C., & Wilson, G. S. (2012). PuffinPlot: A versatile, user-friendly program for paleomagnetic analysis. *Geochemistry, Geophysics, Geosystems*, *13*, Q06Z45. https://doi.org/10.1029/2012GC004098
Meert, J. G., & Santosh, M. (2017). The Columbia supercontinent revisited. *Gondwana Research*, *50*, 67–83. https://doi.org/10.1016/j.gr.2017.04.011
Murthy, G. S. (1978). Paleomagnetic results from the Nain anorthosite and their tectonic implications. *Canadian Journal of Earth Sciences*, *15*(4), 516–525. https://doi.org/10.1139/e78-058
Nordsvan, A. R., Collins, W. J., Li, Z.-X., Spencer, C. J., Pourteau, A., Withnall, I. W., et al. (2018). Laurentian crust in Northeast Australia: Implications for the assembly of the supercontinent Nuna. *Geology*, *46*(3), 251–254. https://doi.org/10.1130/g39980.1
Palmer, H. C., Merz, B. A., & Hayatsu, A. (1977). The Sudbury dikes of the Grenville front region: Paleomagnetism, petrochemistry, and K–Ar age studies. *Canadian Journal of Earth Sciences*, *14*(8), 1867–1887. https://doi.org/10.1139/e77-158
Pearce, J. A. (2008). Geochemical fingerprinting of oceanic basalts with applications to ophiolite classification and the search for Archean oceanic crust. *Lithos*, *100*(1–4), 14–48. https://doi.org/10.1016/j.lithos.2007.06.016
Pei, F., Ye, Y., Wang, F., Cao, H., Lu, S., & Yang, D. (2013). Discovery of Mesoproterozoic diabase dyke in Tonghua region, Jilin Province and its tectonic implications. *Journal of Jilin University (Earth Science Edition)*, *43*(1), 110–118.
Peng, P. (2015). Precambrian mafic dyke swarms in the North China Craton and their geological implications. *Science China Earth Sciences*, *58*(5), 649–675. https://doi.org/10.1007/s11430-014-5026-x
Peng, P., Bleeker, W., Ernst, R. E., Söderlund, U., & McNicoll, V. (2011). U–Pb baddeleyite ages, distribution and geochemistry of 925Ma mafic dykes and 900Ma sills in the North China craton: Evidence for a Neoproterozoic mantle plume. *Lithos*, *127*(1–2), 210–221. https://doi.org/10.1016/j.lithos.2011.08.018
Peng, P., Liu, F., Zhai, M., & Guo, J. (2012). Age of the Miyun dyke swarm: Constraints on the maximum depositional age of the Changcheng system. *Chinese Science Bulletin*, *57*(1), 105–110. https://doi.org/10.1007/s11434-011-4771-x
Peng, P., Wang, X., Windley, B. F., Guo, J., Zhai, M., & Li, Y. (2014). Spatial distribution of ~1950–1800Ma metamorphic events in the North China Craton: Implications for tectonic subdivision of the craton. *Lithos*, *202-203*, 250–266. https://doi.org/10.1016/j.lithos.2014.05.033
Peng, P., Zhai, M., Ernst, R. E., Guo, J., Liu, F., & Hu, B. (2008). A 1.78 Ga large igneous province in the North China craton: The Xiong'er Volcanic Province and the North China dyke swarm. *Lithos*, *101*(3–4), 260–280. https://doi.org/10.1016/j.lithos.2007.07.006
Peng, P., Zhai, M.-G., Li, Q., Wu, F., Hou, Q., Li, Z., et al. (2011). Neoproterozoic (~900Ma) Sariwon sills in North Korea: Geochronology, geochemistry and implications for the evolution of the south-eastern margin of the North China Craton. *Gondwana Research*, *20*(1), 243–254. https://doi.org/10.1016/j.gr.2010.12.011
Peng, T., Wilde, S. A., Fan, W., Peng, B., & Mao, Y. (2013). Mesoproterozoic high Fe–Ti mafic magmatism in western Shandong, North China Craton: Petrogenesis and implications for the final breakup of the Columbia supercontinent. *Precambrian Research*, *235*, 190–207. https://doi.org/10.1016/j.precamres.2013.06.013
Pisarevsky, S. A., Elming, S.-Å., Pesonen, L. J., & Li, Z.-X. (2014). Mesoproterozoic paleogeography: Supercontinent and beyond. *Precambrian Research*, *244*, 207–225. https://doi.org/10.1016/j.precamres.2013.05.014
Pisarevsky, S. A., Wingate, M. T. D., Li, Z.-X., Wang, X.-C., Tohver, E., & Kirkland, C. L. (2014). Age and paleomagnetism of the 1210Ma Gnowangerup–Fraser dyke swarm, Western Australia, and implications for late Mesoproterozoic paleogeography. *Precambrian Research*, *246*, 1–15. https://doi.org/10.1016/j.precamres.2014.02.011
Polat, A., Hofmann, A. W., & Rosing, M. T. (2002). Boninite-like volcanic rocks in the 3.7–3.8 Ga Isua greenstone belt, West Greenland: geochemical evidence for intra-oceanic subduction zone processes in the early Earth. *Chemical Geology*, *184*(3), 231–254. https://doi.org/10.1016/S0009-2541(01)00363-1
Pourteau, A., Smit, M. A., Li, Z.-X., Collins, W. J., Nordsvan, A. R., Volante, S., & Li, J. (2018). 1.6 Ga crustal thickening along the final Nuna suture. *Geology*, *46*(11), 959–962. https://doi.org/10.1130/G45198.1
Rogers, J. J. W., & Santosh, M. (2002). Configuration of Columbia, a Mesoproterozoic supercontinent. *Gondwana Research*, *5*(1), 5–22. https://doi.org/10.1016/s1342-937x(05)70883-2
Seton, M., Müller, R. D., Zahirovic, S., Gaina, C., Torsvik, T., Shephard, G., et al. (2012). Global continental and ocean basin reconstructions since 200Ma. *Earth-Science Reviews*, *113*(3), 212–270. https://doi.org/10.1016/j.earscirev.2012.03.002
Stacey, J. S., & Kramers, J. D. (1975). Approximation of terrestrial lead isotope evolution by a two-stage model. *Earth and Planetary Science Letters*, *26*(2), 207–221. https://doi.org/10.1016/0012-821X(75)90088-6

Stark, J. C., Wang, X.-C., Li, Z.-X., Denyszyn, S. W., Rasmussen, B., & Zi, J.-W. (2018). 1.39 Ga mafic dyke swarm in southwestern Yilgarn Craton marks Nuna to Rodinia transition in the west Australian Craton. *Precambrian Research*, *316*, 291–304. https://doi.org/10.1016/j.precamres.2018.08.014

Su, W., Li, H., Huff, W., Ettensohn, F., Zhang, S., Zhou, H., & Wan, Y. (2010). SHRIMP U-Pb dating for a K-bentonite bed in the Tieling formation, North China. *Chinese Science Bulletin*, *55*(29), 3312–3323.

Sun, S.-S., & McDonough, W.-S. (1989). Chemical and isotopic systematics of oceanic basalts: Implications for mantle composition and processes. *Geological Society, London, Special Publications*, *42*(1), 313–345. https://doi.org/10.1144/GSL.SP.1989.042.01.19

Tarling, D., & Hrouda, F. (1993). *Magnetic Anisotropy of Rocks*. London: Chapman & Hall.

Taylor, S. R. (1964). Abundance of chemical elements in the continental crust: A new table. *Geochimica et Cosmochimica Acta*, *28*(8), 1273–1285. https://doi.org/10.1016/0016-7037(64)90129-2

Van der Voo, R. (1990). The reliability of paleomagnetic data. *Tectonophysics*, *184*(1), 1–9.

Verbaas, J., Thorkelson, D. J., Milidragovic, D., Crowley, J. L., Foster, D., Daniel Gibson, H., & Marshall, D. D. (2018). Rifting of western Laurentia at 1.38 Ga: The Hart River sills of Yukon, Canada. *Lithos*, *316-317*, 243–260. https://doi.org/10.1016/j.lithos.2018.06.018

Wan, B., Windley, B. F., Xiao, W., Feng, J., & Zhang, J. (2015). Paleoproterozoic high-pressure metamorphism in the northern North China Craton and implications for the Nuna supercontinent. *Nature Communications*, *6*, 8344. https://doi.org/10.1038/ncomms9344

Wang, C., Li, Z.-X., Peng, P., Pisarevsky, S., Liu, Y., Kirscher, U., & Nordsvan, A. (2019). Long-lived connection between the North China and north Australian cratons in supercontinent Nuna: Paleomagnetic and geological constraints. *Science Bulletin*, *64*(13), 873–876. https://doi.org/10.1016/j.scib.2019.04.028

Wang, C., Peng, P., Wang, X., & Yang, S. (2016). Nature of three Proterozoic (1680Ma, 1230Ma and 775Ma) mafic dyke swarms in North China: Implications for tectonic evolution and paleogeographic reconstruction. *Precambrian Research*, *285*, 109–126. https://doi.org/10.1016/j.precamres.2016.09.015

Wang, W., Liu, S., Santosh, M., Zhang, L., Bai, X., Zhao, Y., et al. (2015). 1.23 Ga mafic dykes in the North China Craton and their implications for the reconstruction of the Columbia supercontinent. *Gondwana Research*, *27*(4), 1407–1418. https://doi.org/10.1016/j.gr.2014.02.002

Wang, Y., Zhao, G., Fan, W., Peng, T., Sun, L., & Xia, X. (2007). LA-ICP-MS U–Pb zircon geochronology and geochemistry of Paleoproterozoic mafic dykes from western Shandong Province: Implications for back-arc basin magmatism in the eastern block, North China Craton. *Precambrian Research*, *154*(1–2), 107–124. https://doi.org/10.1016/j.precamres.2006.12.010

Winchester, J. A., & Floyd, P. A. (1977). Geochemical discrimination of different magma series and their differentiation products using immobile elements. *Chemical Geology*, *20*, 325–343. https://doi.org/10.1016/0009-2541(77)90057-2

Wingate, M. T. D., & Compston, W. (2000). Crystal orientation effects during ion microprobe U–Pb analysis of baddeleyite. *Chemical Geology*, *168*(1), 75–97. https://doi.org/10.1016/S0009-2541(00)00184-4

Xiang, Z. (2014). Mesoproterozoic Magmatic Events and Mineralization in the North China Craton. *(Doctoral dissertation)*. Beijing: China University of Geosciences (Beijing).

Xu, Y., Chung, S.-L., Jahn, B.-m., & Wu, G. (2001). Petrologic and geochemical constraints on the petrogenesis of Permian–Triassic Emeishan flood basalts in southwestern China. *Lithos*, *58*(3), 145–168. https://doi.org/10.1016/S0024-4937(01)00055-X

Yang, J., Wu, F., Liu, X., & Xie, L. (2005). Zircon U–Pb ages and Hf isotopes and their geological significance of the Miyun rapakivi granites from Beijing, China. *Acta Petrologica Sinica*, *21*(6), 1633–1644.

Yang, K.-F., Fan, H.-R., Santosh, M., Hu, F.-F., & Wang, K.-Y. (2011). Mesoproterozoic mafic and carbonatitic dykes from the northern margin of the North China Craton: Implications for the final breakup of Columbia supercontinent. *Tectonophysics*, *498*, 1–10. https://doi.org/10.1016/j.tecto.2010.11.015

Zhai, M. (2011). Cratonization and the Ancient North China continent: A summary and review. *Science China Earth Sciences*, *54*(8), 1110–1120.

Zhai, M.-G., & Santosh, M. (2011). The early Precambrian odyssey of the North China Craton: A synoptic overview. *Gondwana Research*, *20*(1), 6–25. https://doi.org/10.1016/j.gr.2011.02.005

Zhang, S., Li, Z.-X., Evans, D. A. D., Wu, H., Li, H., & Dong, J. (2012). Pre-Rodinia supercontinent Nuna shaping up: A global synthesis with new paleomagnetic results from North China. *Earth and Planetary Science Letters*, *353-354*, 145–155. https://doi.org/10.1016/j.epsl.2012.07.034

Zhang, S., Zhao, Y., Ye, H., Hu, J., & Wu, F. (2013). New constraints on ages of the Chuanlinggou and Tuanshanzi formations of the Changcheng system in the Yan-Liao area in the northern North China Craton. *Acta Petrologica Sinica*, *29*(7), 2481–2490.

Zhang, S.-H., Liu, S.-W., Zhao, Y., Yang, J.-H., Song, B., & Liu, X.-M. (2007). The 1.75–1.68 Ga anorthosite-mangerite-alkali granitoid-rapakivi granite suite from the northern North China Craton: Magmatism related to a Paleoproterozoic orogen. *Precambrian Research*, *155*(3–4), 287–312.

Zhang, S.-H., Zhao, Y., Li, X.-H., Ernst, R. E., & Yang, Z.-Y. (2017). The 1.33–1.30 Ga Yanliao large igneous province in the North China Craton: Implications for reconstruction of the Nuna (Columbia) supercontinent, and specifically with the north Australian Craton. *Earth and Planetary Science Letters*, *465*, 112–125. https://doi.org/10.1016/j.epsl.2017.02.034

Zhang, S.-H., Zhao, Y., & Santosh, M. (2012). Mid-Mesoproterozoic bimodal magmatic rocks in the northern North China Craton: Implications for magmatism related to breakup of the Columbia supercontinent. *Precambrian Research*, *222-223*, 339–367. https://doi.org/10.1016/j.precamres.2011.06.003

Zhang, S.-H., Zhao, Y., Ye, H., & Hu, G.-H. (2016). Early Neoproterozoic emplacement of the diabase sill swarms in the Liaodong peninsula and pre-magmatic uplift of the southeastern North China Craton. *Precambrian Research*, *272*, 203–225. https://doi.org/10.1016/j.precamres.2015.11.005

Zhao, G., Cawood, P. A., Li, S., Wilde, S. A., Sun, M., Zhang, J., et al. (2012). Amalgamation of the North China Craton: Key issues and discussion. *Precambrian Research*, *222-223*, 55–76. https://doi.org/10.1016/j.precamres.2012.09.016

Zhao, G., Cawood, P. A., Wilde, S. A., & Sun, M. (2002). Review of global 2.1–1.8 Ga orogens: Implications for a pre-Rodinia supercontinent. *Earth-Science Reviews*, *59*, 125–162. https://doi.org/10.1016/S0012-8252(02)00073-9

Zhao, T., Chen, F., Zhai, M., & Xia, B. (2004). Single zircon U-Pb ages and their geological significance of the Damiao anorthosite complex, Hebei Province, China. *Acta Petrologica Sinica*, *20*(3), 685–690.

Zhao, T., Zhai, M., Xia, B., Li, H., Zhang, Y., & Wan, Y. (2004). Zircon U-Pb SHRIMP dating for the volcanic rocks of the Xiong'er group: Constraints on the initial formation age of the cover of the North China Craton. *Chinese Science Bulletin*, *49*(23), 2495–2502. https://doi.org/10.1007/bf03183721

Zhao, T., Zhu, G., Lin, S., & Wang, H. (2016). Indentation-induced tearing of a subducting continent: Evidence from the Tan–Lu Fault Zone, East China. *Earth-Science Reviews*, *152*, 14–36. https://doi.org/10.1016/j.earscirev.2015.11.003